POLITECNICO DI MILANO
Corso di Laurea Magistrale in Ingegneria Chimica
Dipartimenti di Chimica, Materiali e Ingegneria Chimica "Giulio Natta"

Tesi di Laurea Magistrale

Low-T_g Polymeric Latices for Liquid Waterproofing Polymer-Cement Membranes

Relatore:
Prof. Dr. Massimo Morbidelli

Correlatore:
Dr. Stefano Caimi

Tesi di:
Michela Banfi
matricola 875578

Anno Accademico 2017-2018

Acknowledgements

First of all, I would like to express my sincere gratitude to Prof. Dr. Massimo Morbidelli for giving me the opportunity to carry out my thesis project in his research group at ETH Zürich.

A huge thank goes to my daily supervisor Stefano, for his untiring enthusiasm and extreme patience. For passing me on the passion for the lab work and for teaching me everything I needed to get confident with the project. (And last, thanks for opening the tight-closed bottles!)

Many thanks to the whole Morbidelli group for the hospitality, and in particular to Elias and Dario for sharing the working hours in the laboratory during the first part of my stay, to Antoine for the SEM images, and to Vasco and Vanni for the many (and absolutely needed) coffee breaks and for all the nice moments we shared.

A great thanks to Roger and all the KTI project team, for sharing interesting meetings and giving useful hints about this research.

Last but not least, an endless thank goes to my family for always sustaining me and for making it possible to spend these months in Zürich, and to Alberto, for his untiring support and for always believing in me, especially when I didn't.

Table of contents

Abstract

One-component polymer-cement mortars systems represent the new frontier in waterproofing construction materials, combining high-performances and excellent durability with low costs and a low environmental impact. In order to ensure crack-bridging and waterproofing properties even at severe temperature conditions, a low-T_g copolymer has to be synthesized. In particular, to fulfill the one-component system requirements, latices able to be spray-dried and consequently redispersed need to be studied. For this purpose, two different systems were considered. Specifically, latices exposing carboxyl groups onto the particles surface and core-shell particles constituted by a soft core and a hard shell have been synthesized and characterized. More precisely, the effect that different types and percentages of acid and different shell compositions and thicknesses have on the spray-drying and crack-bridging properties was investigated. Both the configurations showed a limited particles coalescence and coagulation during the drying phase, leading to fine-grain sized powders redispersible in water by simple stirring, thus proving their applicability in dry-mix composite materials. In particular, in the case of the addition of carboxyl groups, the best performing type and percentage of acid was shown to be 1% acrylic acid. On the other hand, in the case of core-shell particles, it was observed that although a thicker shell improves the spray-ability, crack-bridging properties of the produced membrane result lower. A systematic study of the core-shell morphology showed that a trade-off between spray-ability and crack-bridging is the key for the optimal polymer nanoparticles design. Final studies merging the two particle configurations are also proposed, opening the way to possible future promising studies.

Abstract in lingua italiana

Le malte monocomponente polimero-cemento rappresentano la nuova frontiera dei materiali da costruzione impermeabilizzanti, coniugando alte prestazioni ed eccellente durata con bassi costi e basso impatto ambientale. Al fine di garantire le proprietà di impermeabilità e resistenza a frattura anche a basse temperature, è necessario sintetizzare un copolimero caratterizzato da una bassa temperatura di transizione vetrosa (T_g). In particolare, per soddisfare i requisiti derivanti da un sistema monocomponente, è necessario studiare lattici in grado di essere essiccati a spruzzo e in seguito ridispersi. A tal fine sono stati presi in considerazione due sistemi diversi. In particolare, sono stati sintetizzati e caratterizzati lattici che espongono gruppi carbossilici sulla superficie e particelle costituite da un nucleo morbido e da un guscio duro. Più precisamente, è stato studiato l'effetto che diversi tipi e percentuali di acidi e diverse composizioni e spessori del guscio hanno sull'atomizzazione e sulla resistenza a frattura. Entrambe le configurazioni hanno mostrato una limitata coalescenza e coagulazione delle particelle durante la fase di essiccamento, che ha portato a polveri a grana fine ridisperdibili in acqua per semplice agitazione, dimostrando così la loro applicabilità nei materiali compositi costituiti da una miscela di diverse polveri cementizie. In particolare, nel caso dell'aggiunta di gruppi carbossilici, il tipo e la percentuale di acido più performante è rappresentata dall'1% di acido acrilico. D'altra parte, nel caso delle particelle nucleo-guscio, è stato osservato che, sebbene un guscio più spesso migliora l'operazione di essiccamento, le proprietà di resistenza a frattura della membrana prodotta risultano inferiori. Uno studio sistematico della morfologia di particelle caratterizzate da una struttura nucleo-guscio ha dimostrato che il compromesso tra la capacità di essiccamento e la resistenza a frattura è la chiave per la progettazione ottimale delle nanoparticelle polimeriche. Vengono inoltre proposti studi finali che uniscono le due configurazioni di particelle, aprendo la strada a possibili promettenti studi per il futuro.

List of Figures

List of Tables

List of Abbreviations and Symbols

$1C$	one-component system
$2C$	two-component system
$2\text{-}EHA$	2-ethylhexyl acrylate
A	cross sectional area of the drying chamber
AA	acrylic acid
API	active pharmaceutical ingredients
Bi	Biot number
C_p^L	specific heat of the liquid phase
CF	monomer mixture to be fed
D	particle diffusion coefficient
D_P	diameter of the particle
DLS	dynamic light scattering
DSC	differential scanning calorimetry
dV	control volume
h	heat transfer coefficient
$\dot{H}$	enthalpy flux
$\dot{H}_{ev}$	heat flux due to the evaporation of the liquid phase
h_{liq}^P	enthalpy of the liquid phase in the particle
h_{vap}^P	enthalpy of the vapor phase in the particle
I	initiator
$I\bullet$	initiator radical
IC	initial charge
IF	remaining initiator solution to be fed
IS	initiator solution
J_{CONV}^{tot}	convective mass flux
J_{TH}^{tot}	convective thermal flux
k	thermal conductivity
k_1	rate constant of initiator reacting with monomer
k_B	Boltzmann constant, $1.381 \cdot 10^{-23}$ J/K
k_{conv}	coefficient for the convective exchange
k_{ct}	chain transfer rate constant
k_d	initiator decomposition rate constant
k_{ij}	rate constant of propagating radical chain with monomer *i* at the end reacting with monomer *j*
k_P	propagation rate constant

k_t	termination rate constant
k_{tc}	termination by combination rate constant
k_{td}	termination by disproportion rate constant
μ	viscosity of the medium
M	monomer
M_i	monomer *i*
[M]	concentration of the monomer
$[M_i]$	concentration of monomer *i*
m_i	instantaneous concentration of monomer *i* in the growing polymer chain
$M\bullet_i$	propagating radical chain with monomer *i* at the end
$[M\bullet_i]$	concentration of propagating radical chain with monomer *i* at the end
$\dot{m}_P^{tot}$	particles mass flux
m_P	mass of the particle
MAA	methacrylic acid
MMA	methyl methacrylate
MAPTAC	[3-(Methacryloylamino)propyl]trimethylammonium chloride solution
MFFT	minimum film-forming temperature
NMR	nuclear magnetic resonance
P_i	terminated polymer chain
P_w	partial pressure of water
$P°(T_P)$	vapor pressure of the water at the particle temperature
ΔP	pressure gradient
PCMs	polymer-cement mortars
PDI	polydispersity index
PvOH	polyvinyl alcohol
$R\bullet_i$	propagating radical chain
$[R\bullet_i]$	radical concentration
r	particle radius
r_1	reactivity ratio of monomer 1
r_2	reactivity ratio of monomer 2
r_i	rate of initiation
r_p	rate of propagation
r_t	rate of termination
RPPs	redispersible polymer powders
S	chain transfer agent
S_P	particle surface area
SEM	scanning electron microscopy
SF	shell feed
STY	styrene

$t_{1/2}$	time of half-life
T_g	glass transition temperature
T_{hg}	temperature of the hot gas
T_m	melting temperature
T_P	temperature of water in the solid
ΔT	temperature gradient
v_P	velocity of the particle
ω_{m_i}	weight fraction of the monomer *i*
WT	waiting time
ζ	zeta
z	axial coordinate

1. Introduction

1.1 Polymeric latex

A polymeric latex is defined as a colloidal dispersion of polymer particles in an aqueous medium, also referred to as polymeric dispersion or water-borne latex.[1, 2]
It is composed of nano-sized polymer particles (typically 100 nm) dispersed in water and, prior processing, it appears as a milky fluid. Polymeric dispersions are widely used in many varied applications such as synthetic rubbers, paints, adhesives, additives for construction materials, additives in paper and textile industries, and leather treatment.[1-7] The growing use of these materials is due to several factors: i) it is more and more necessary to replace solvent-borne systems with water-borne ones because of environmental concerns and governmental regulations; ii) the unique properties of polymeric dispersions allow to satisfy a wide range of application requirements; iii) the polymerization in dispersed media ensures a better operating control compared with other polymerization processes.[3] Nowadays, latices are mostly obtained by free-radical polymerization, and in particular by emulsion polymerization.[4]

1.2 Principles of radical chain polymerization

Polymer synthesis reactions, also referred to as polymerizations, can be divided in step and chain polymerizations. Step polymerizations consist in a step-wise reaction between functional groups of monomeric reactants. Their size increases slowly and proceeds from monomer to dimer, trimer, tetramer, and so on. This reaction occurs between any species in the system. Conversely, chain polymerizations rely on the presence of a reactive center belonging to an initiator, which might be a free-radical, an anion or a cation. In this case, the monomer is reacting with the active center, thus growing the polymer chain and simultaneously regenerating the active center itself. In this case, the monomer does not react with differently sized polymer species and throughout the reaction there are only long polymer chains and monomer species present.[5]
Radical chain polymerizations consist of four sequential steps:

- Initiation: in this step an initiator decomposes to give free-radicals

$$I_2 \xrightarrow{k_d} I\bullet + I\bullet \quad (1)$$

$$I\bullet + M \xrightarrow{k_1} R\bullet_1 \quad (2)$$

where k_d is the decomposition rate constant of the initiator and k_1 is the rate constant of the reaction between the radical and the monomer, forming a new radical.

- Propagation: this step consists in the addition of a monomer to the growing polymer chain

$$R\bullet_n + M \xrightarrow{k_P} R\bullet_{n+1} \quad (3)$$

where k_P is the rate constant of the propagation reaction.

- Chain transfer: in this step the reactive radical center is moved from the growing polymer chain to another molecule, stopping in this way the growth of the first polymer chain. This mechanism can be induced by the addition of a chain transfer agent

$$R\bullet_n + S \xrightarrow{k_{ct}} R\bullet_1 + P_n \quad (4)$$

or it can occur as a side reaction, where the radical can be transferred either to a monomer

$$R\bullet_n + M \xrightarrow{k_{ct}} R\bullet_1 + P_n \quad (5)$$

or to another polymer chain

$$R\bullet_n + P_m \xrightarrow{k_{ct}} R\bullet_m + P_n \quad (6)$$

This last mechanism occurs especially at high conversions, when the polymer content is sufficiently high.

- Termination: this final step consists in the recombination of two radicals and leads to the production of a terminated (dead) polymer species. It can be caused by combination, when two active chains combine

$$R\bullet_n + R\bullet_m \xrightarrow{k_{tc}} P_{n+m} \quad (7)$$

or by disproportion, when two radical chains terminate while preserving their identity, thus forming two dead polymer chains:

$$R\bullet_n + R\bullet_m \xrightarrow{k_{td}} P_n + P_m \quad (8)$$

The polymerization rate can be calculated by assuming k_P, k_{tc} and k_{td} as constant throughout the reaction, thus considering all the rate constants independent of the radical chain size. This is reasonable when working in a solvent (as the system viscosity remains low all along the reaction) and because the influence of the size on the rate constants decreases very rapidly, becoming negligible already at trimer size.[6] As the monomer concentration changes due to initiation (Equation (2)) or to propagation (Equation (3)), the rate of polymerization can be written as

$$-\frac{d[M]}{dt} = r_i + r_p \tag{9}$$

where r_i and r_p are respectively the rate of initiation and the rate of propagation. By considering that there are far more monomer molecules reacting by propagation than by initiation, r_i can be neglected. This assumption results in considering the rate of polymerization equal to the rate of propagation

$$-\frac{d[M]}{dt} = r_p = k_P[R\bullet][M] \tag{10}$$

The radical concentration can be assumed at steady-state conditions. This assumption allows considering the rate of initiation r_i the same as the one of termination r_t

$$r_i = r_t = 2k_t[R\bullet]^2 \tag{11}$$

Equation (11) can be rearranged and substituted in Equation (10), obtaining the final polymerization rate

$$r_p = k_P[M]\left(\frac{r_i}{2k_t}\right)^{1/2} \tag{12}$$

1.3 Copolymerization

Copolymers are polymers made of two or more monomers. Their synthesis allows tuning the properties of the final material quite freely, playing with the distribution of different monomer units inside the chains. Generally, this technique is used to modify polymer properties such as crystallinity, flexibility, melting temperature and glass transition temperature.[5] According to the method used for the copolymer synthesis, different chain architectures are obtained. A random copolymer is characterized by a linear structure in which the different monomers are distributed randomly. An alternating copolymer has alternating monomeric units in equimolar amounts in a linear structure. A block copolymer

is constituted by a linear structure with uninterrupted sequences of the same monomeric units, while graft copolymers have a backbone of one monomer where one or more side chains of the other monomer are attached (see Figure 1).[5]

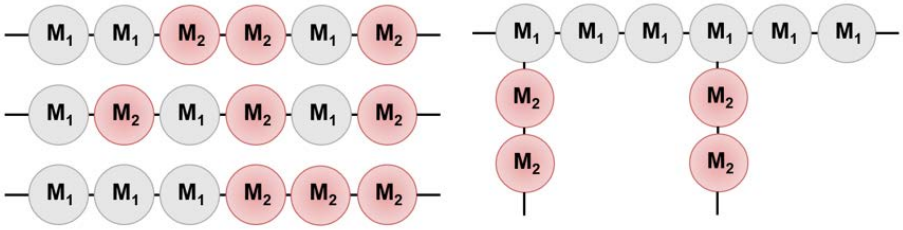

Figure 1. Comparison between a random copolymer (top left), an alternating copolymer (middle left), a block copolymer (bottom left) and a nonlinear graft copolymer (right).

The magnitude of the property alterations differs depending on the type of structure involved. The different structures and the monomer distribution of the resulting copolymer depend on the synthesis technique, the feed composition as well as the reactivity of the monomers involved. For instance, under specific conditions, the first addition of one monomer into the reactor and the subsequent addition of a second one into the radical chain leads to a block copolymer. On the other hand, a random copolymer is synthetized by adding both monomers simultaneously and a graft copolymer requires special synthesis conditions. For the purpose of this work, relevance is given only to random copolymers. Often, when synthesizing a random copolymer, the instantaneous copolymer composition does not resemble the feed composition. This occurs because different monomers have a different tendency to react with the growing polymer chains, thus they may react with a monomer or another. In the same way, the copolymerization rates cannot be assessed by simply knowing the rates of homopolymerization of the respective single monomers. In general, a copolymerization with two monomers M_1 and M_2 involves two propagating radical species $M\bullet_1$ and $M\bullet_2$ and it is characterized by the same steps of a radical chain homopolymerization. However, as each monomer can react with each of the two radicals, there are four possible chain propagation reactions:

$$M\bullet_1 + M_1 \xrightarrow{k_{11}} M\bullet_1 \tag{13}$$

$$M\bullet_1 + M_2 \xrightarrow{k_{12}} M\bullet_2 \tag{14}$$

$$M\bullet_2 + M_1 \xrightarrow{k_{21}} M\bullet_1 \tag{15}$$

$$M\bullet_2 + M_2 \xrightarrow{k_{22}} M\bullet_2 \tag{16}$$

When a radical reacts with a monomer of the same type, the reaction is called homopropagation, as in the case of Equation (13) and (16). On the other hand, when a radical reacts with the other type, as in Equation (14) and (15), it is defined cross-propagation. Assuming that the main consumption of monomer is due to the propagation reactions, the variation of the monomer concentrations in time can be written as

$$-\frac{d[M_1]}{dt} = k_{11}[M\bullet_1][M_1] + k_{21}[M\bullet_2][M_1] \tag{17}$$

$$-\frac{d[M_2]}{dt} = k_{22}[M\bullet_2][M_2] + k_{12}[M\bullet_1][M_2] \tag{18}$$

Because radicals are very reactive, their composition can be assumed as constant in time (pseudo steady-state assumption), so that

$$\frac{d[M\bullet_1]}{dt} = \frac{d[M\bullet_2]}{dt} = 0 \tag{19}$$

In order to make the concentration of the radical species constant, the rate of their interconversion must be equal

$$k_{21}[M\bullet_2][M_1] = k_{12}[M\bullet_1][M_2] \tag{20}$$

By dividing Equation (17) by Equation (18)

$$\frac{d[M_1]}{d[M_2]} = \frac{[M_1]}{[M_2]} \cdot \frac{k_{11}[M\bullet_1]+k_{21}[M\bullet_2]}{k_{22}[M\bullet_2]+k_{12}[M\bullet_1]} \tag{21}$$

Which can be further simplified by using Equation (20) into

$$\frac{d[M_1]}{d[M_2]} = \frac{[M_1]}{[M_2]} \cdot \frac{\frac{k_{11}}{k_{12}}\cdot[M_1]+[M_2]}{\frac{k_{22}}{k_{21}}\cdot[M_2]+[M_1]} \tag{22}$$

This last equation describes the rate of incorporation of monomers M_1 and M_2 into the polymer chain. By introducing the reactivity ratios $r_1 = \frac{k_{11}}{k_{12}}$ and $r_2 = \frac{k_{22}}{k_{21}}$, the chain polymerization equation (Equation (22)) can be rewritten as

$$\frac{d[M_1]}{d[M_2]} = \frac{m_1}{m_2} = \frac{[M_1]}{[M_2]} \cdot \frac{r_1\cdot[M_1]+[M_2]}{r_2\cdot[M_2]+[M_1]} \tag{23}$$

where m_1 and m_2 stand for the instantaneous concentration of M_1 and M_2 in the polymer. Due to the so-called composition drift, the instantaneous concentration can be different at varying conversions. This phenomenon leads to the preferred incorporation of one monomer at a certain conversion and will change as the bulk concentration of the more reactive monomer decreases. For a binary copolymerization reaction, this behavior is fully characterized by reactivity ratios and monomer concentrations, in agreement with Equation (23). According to the value assumed by the reactivity ratio, the radical reacts preferably with one monomer rather than another. For instance, $r_1 = 0$ means that M_1 cannot undergo homopolymerization. For $0 < r_1 < 1$, $M\bullet_1$ prefers to react with M_2, while $r_1 > 1$ means that $M\bullet_1$ prefers to react with M_1. In the case of binary copolymerization reactions, it is possible to distinguish four cases:

- $r_1 < 1 \wedge r_2 < 1$: monomers tend to heteropolymerize in a random copolymerization where a composition drift can occur. Depending on the feed composition, one of the two monomers is preferably incorporated. When a certain feed composition is used, the equality $\frac{m_1}{m_2} = \frac{[M_1]}{[M_2]}$ becomes valid, therefore the feed composition is equal to the instantaneous polymer composition. This point is called azeotropic point.

- $r_1 = r_2 = 1$: the incorporation of both monomers proceeds with the same growing chain rate, therefore the instantaneous polymer composition is similar to the feed composition. This is called ideal copolymerization.

- $r_1 < 1 \wedge r_2 > 1$ or $r_1 > 1 \wedge r_2 < 1$: the incorporation of one of the two monomers is preferred over the other. In this case composition drift could occur as well.

- $r_1 = r_2 = 0$: a chain end will always incorporate the respective other monomer. This case gives rise to an alternating copolymer.

Composition drift can be readily detected by plotting the instantaneous composition of the copolymer as a function of the composition of the corresponding monomer mixture (Figure 2). For instance, in the case of a copolymerization involving styrene and 2-ethylhexyl acrylate, the respective reactivity ratios are $r_1 = 0.96$ and $r_2 = 0.31$.[8] Therefore, reminding the cases described above, this situation leads to a random copolymer. In this case, the azeotropic point corresponds to a monomer mixture molar composition of 0.95. Therefore, if the styrene content of the monomer mixture is smaller than this value, the corresponding instantaneous copolymer composition will be larger than 0.95, with preferred incorporation of styrene. Accordingly, the residual monomer mixture will become

less rich in styrene, thus producing copolymer chains getting poorer in styrene and richer in 2-ethylhexyl acrylate. In order to prevent this composition drift, which is unwanted when copolymers with uniform composition are desired, the reaction is run in semi-batch mode under starved conditions. Under these conditions, the monomer feed rate is slower than the actual polymerization rate, and the system has no other possibility than incorporating into the polymer the available monomer mixture. In this way, the composition of monomers in the reactor stays constant throughout the reaction and so does the copolymer composition.[9, 10]

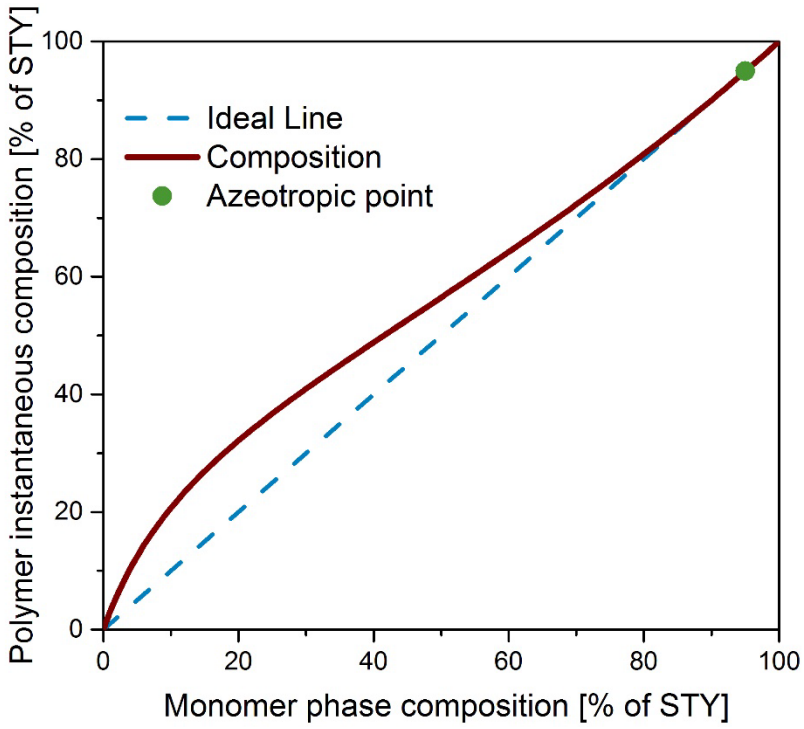

Figure 2. Mayo-Lewis plot for the copolymerization of styrene and 2-ethylhexyl acrylate.

1.4 Emulsion polymerization

Emulsion polymerization is nowadays an important polymerization process, representing about 10% of the overall polymer production. The final product can be used as water dispersion, and this is the case for paints and coatings (26%), paper coating (23%), adhesives (22%), and carper backing (11%). On the other hand, the produced polymers can be also recovered as dry powder (18%), to be used for tires, electrical and electronic equipments, automotive, and housing. The fast development of this reaction was due to both the possibility of producing a high molecular weight colloidal polymer with unique properties and the need to replace solvent-based systems with water-borne products, imposed by governmental regulations and environmental concerns. Furthermore, the wide use of this

process is justified by the versatility of the reaction, the ease of heat removal and the ability to control the properties of the produced polymers.[4, 7]

1.4.1 Main ingredients

A typical formulation of an emulsion polymerization is composed of four ingredients: 1) the dispersing medium, 2) the monomer(s), 3) the initiator, and 4) the stabilizer. Further auxiliaries, such as buffers, co-solvents, chain transfer agents, *etc*., can be used to improve the properties of the produced latex.[11]

Dispersion medium
The dispersion medium is represented by water, which provides a cheap, nontoxic, nonflammable, and environmentally friendly system. It is an excellent heat transfer medium and has low viscosity. Furthermore, it represents the medium through which monomer transfers from droplets to particles and the solvent for initiator and (partly) stabilizers.

Monomer
Emulsion polymerization requires the presence of free-radical polymerizable monomers, which form the structure of the polymer itself. Monomers suitable for this kind of synthesis have been divided in three groups.[12] Depending on the group the monomer belongs to, the synthesis will have different characteristics.
The first group consists of monomers with relatively good solubility in water (around 8%). Polymerization begins in the aqueous solution containing the monomer and it is further continued in the polymer-monomer particles deriving from the macromolecules precipitating in the aqueous solution and from the polymer radicals.
The second group comprises the monomers with low solubility in water (approximately 1-3%). This is the case of methyl methacrylate and other acrylates. The polymer formation begins in the aqueous solution or in micelles of emulsifier and proceeds in polymer-monomer particles deriving from the micelles and the macromolecules precipitating out of the aqueous solution.
The third group includes monomers almost insoluble in water. Belonging to this group are monomers like styrene, butadiene, vinyl chloride, *etc*. In this case, polymerization begins in the micelles of the stabilizing agent and continues in polymer-monomer particles formed from micelles.
A typical formulation of emulsion polymerization includes monomers that present low water solubility, even though combinations of monomers with low and high water solubility are frequently used.

Initiator

The function of the initiator in emulsion polymerization is to produce radicals upon decomposition. The generated free-radicals will then lead to the propagation of the polymer molecules. The production of free-radicals can occur *via* two different mechanisms: thermal decomposition and redox reactions. The difference between the two types of initiator is dictated by the temperature at which the process is carried out: thermal initiators are used for high temperature processes (50-90 °C), while redox systems are used when lower temperatures are required.

Generally, also light and other types of radiation can be used to generate free-radicals. However, they are not commonly used in emulsion polymerization.

The main initiators and the respective free-radicals produced by thermal decomposition or redox reaction are:[4, 13]

1. Persulfates

$$S_2O_8^{-2} \rightarrow SO_4\bullet^{-1} + SO_4\bullet^{-1}$$

2. Hydrogen peroxides

$$HO - OH \rightarrow HO\bullet + HO\bullet$$

3. Organic peroxides

$$RO - OR' \rightarrow RO\bullet + R'O\bullet$$

4. Azo compounds

$$RN = NR' \rightarrow R\bullet + R'\bullet + N_2$$

5. Persulfate-Bisulfite

$$S_2O_8^{-2} + HSO_3^{-1} \rightarrow SO_4\bullet^{-1} + SO_3\bullet^{-1} + HSO_4^{-1}$$

The rate of decomposition of each initiator is specified by its "half-life" which is defined as the time required to halve its concentration at a given temperature. The value of $t_{1/2}$ changes according to the type of initiator and decreases with the increase of temperature. Assuming the decomposition to proceed *via* a first order kinetics reaction (which normally happens for most free-radical initiators), the half-time is related to the decomposition rate of the initiator (k_d) by the following relation:

$$t_{1/2} = \frac{ln2}{k_d} \tag{24}$$

Stabilizers

These compounds play an important role in the production and application of latices because of the many functions they perform during emulsion polymerization. Indeed, they are responsible for: i) the formation of micelles, due to aggregation of surfactant molecules, when the concentration exceeds the critical micellar concentration in the aqueous system, ii) the facilitation of particles nucleation, iii) the stabilization of the monomer droplets, and iv) the stabilization of the polymer particles during polymerization.[4] In particular, the presence of a stabilizer in the polymerization recipe is essential to control the particle size and the stability of the latex.[14] Stabilizers can be divided in two main groups: reactive and unreactive surfactants.[15] Although the use of unreactive surfactants is very common, they have some adverse effects that make the reactive surfactants preferable.[5, 14-21] In fact, as the unreactive surfactants are not covalently bound onto the particle surface, they can migrate on and eventually desorb from the particle surface, thus losing their stabilization effect. Such desorption can take place by competitive adsorption as well as when the latex is subjected to very high shear. In addition, surfactant behavior influences also the latex film-formation, a characteristic needed for the project application, as will be explained later on. In particular, when the film is exposed to water or high humidity, it shows lack of adhesiveness and low-dimensional stability due to phase separations induced by the unreactive surfactant.[14] Conversely, the use of reactive surfactants ensures that the stabilizer molecules are chemically bound onto the polymer particles, avoiding, in this way, their consequent desorption and/or migration.[19, 21]

Reactive surfactants owe their name to the fact that they participate in one of the chemical reactions involved in the polymerization. They are named differently according to the way they behave during the reaction: *inisurf*, if the surfactant acts as both initiator and stabilizer, *transurf* if it behaves both as transfer agent and stabilizer, or *surfmer* when it acts both as co-monomer and stabilizer.[14, 18] This work deals with the use of surfmers, a combination of surfactant and monomer. Thanks to the presence of a polymerizable double bond inside its structure, the surfmer can react with, and therefore is covalently bound to, the polymer, with no possibility of movement or desorption.[16, 19] Furthermore, Tauer *et al*.[22] showed that the use of a surfmer helps to obtain a latex with lower surface tension, thus helping the redispersibility of the polymer powder. In order to exploit at its best the property of these compounds, Schoonbrood *et al*.[19] reviewed the two key aspects of the surfmer behavior in order to ensure best performances: (i) the surfmer should not react during the initial stage of the polymerization reactions, when the particle can increase significantly in size, burying the surfactant groups inside, and (ii) it should react to completion in the final stages, when the particles have almost reached their final size, so that it can be mainly incorporated on the particles surface.

Other ingredients

In addition to the main abovementioned ingredients, a wide variety of additives may be included in the formulation of emulsions to enhance the performance and the properties of the final product. Some examples of possible additives are listed below.

Buffers, usually $CaCO_3$, $NaHCO_3$ or Na_2CO_3, are added to regulate the pH of the system. *Chain transfer agents*, such as aldehydes, amines and disulfides, are used to regulate the distribution of the molar mass of the latex and the molecular weight development in the emulsion. *Cross-linking agents* are added to enhance the shear strength and to confer the adequate tack to the latices. Last but not least, additional *functional monomers* are often added to the emulsion recipe to improve the final properties. This is the case of acrylic acid (AA) and methacrylic acid (MAA) (Figure 3), which are often used for the production of coatings, floor polish, inks and adhesives.[5, 23]

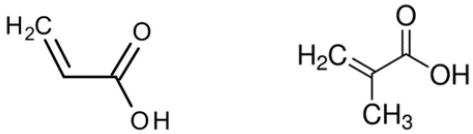

Figure 3. Chemical structure of AA and MAA.

1.4.2 The mechanism

Emulsion polymerization is a process that proceeds *via* radical addition polymerization in a heterogeneous system. The kinetic mechanism of emulsion polymerization is typically divided in three intervals.

- Interval I (also referred to as nucleation) – the monomer is present inside the system in three different ways: dissolved in water, absorbed in the micelles and dispersed in droplets. At the very beginning of the reaction, the radicals produced by the decomposition of the initiator in the aqueous phase are too hydrophilic to enter directly the organic phase, and for this reason they react with the monomer dissolved in the aqueous system creating oligoradicals. In this step, the growth rate of the oligoradicals is generally very low due to the low concentration of monomer dissolved in water. When the oligoradicals reach a certain chain length, they become too hydrophobic to remain in the aqueous phase and diffuse into the organic phase, represented by both the micelles and the monomer droplets.[7] The choice to enter one or the other system depends upon the surface area available for diffusion. As the micelles specific area is about three orders of magnitude greater than the one of the droplets, most of radicals enter the micelles.[24] As only a negligible amount of radicals enters the droplets, it is possible to assume that there is no reaction inside the droplets.[25] The entrance of the radicals inside the micelles is considered the

very beginning of Interval I. Thanks to the monomer-rich environment encountered inside the micelles, the growth of oligoradicals proceeds very fast and the micelle becomes a polymer particle. Nucleation phase is characterized by the simultaneous presence of monomer droplets, monomer swollen micelles and monomer swollen polymer particles inside the reactor. Polymer particles increase in number during the nucleation time and become the main polymerization *loci*. Monomer droplets supply the monomer consumed inside the polymer particle by diffusion through the aqueous phase (Figure 4), to reestablish the chemical equilibrium. Therefore, while the polymer particles increase in size, the monomer droplets become smaller. In the same way, the number of micelles in the system decreases as they are transformed into polymer particles. Furthermore, the nucleated polymer particle adsorbs the surfactant available in the aqueous phase, until all the micelles disappear. The complete disappearance of the micelles marks the end of the nucleation phase.

- Interval II (also referred to as growth) – it is characterized by the presence of only monomer droplets and monomer swollen polymer particles. In this phase, the number of polymer particles remains constant, but their volume increases in time because of polymerization and monomer transport. During this interval, monomer droplets become progressively smaller, due to the diffusion of the monomer from the droplets to the polymer particles through the water phase. The disappearance of monomer droplets marks the end of Interval II. At the end of this interval, the conversion of the monomer is still quite low: for instance, 40% conversion for styrene and 15% conversion for vinyl acetate, for a typical reaction reported in the literature.[26] This is because the monomer conversion depends on the amount of monomer swollen into the polymer particles. The disappearance of monomer droplets depends on the maximum swelling, the higher this is, the earlier the droplets disappear. Thus, as the swelling is directly proportional to the water solubility of the monomer, the more water-soluble the monomer, the lower the conversion at the end of Interval II. As a consequence, most of the monomer polymerizes in Interval III.

- Interval III (also referred to as monomer depletion) – in this interval the polymerization proceeds in the polymer particles. Here, the monomer concentration decreases continuously and so does the rate of polymerization, which decreases towards the end of the process.[24, 26]

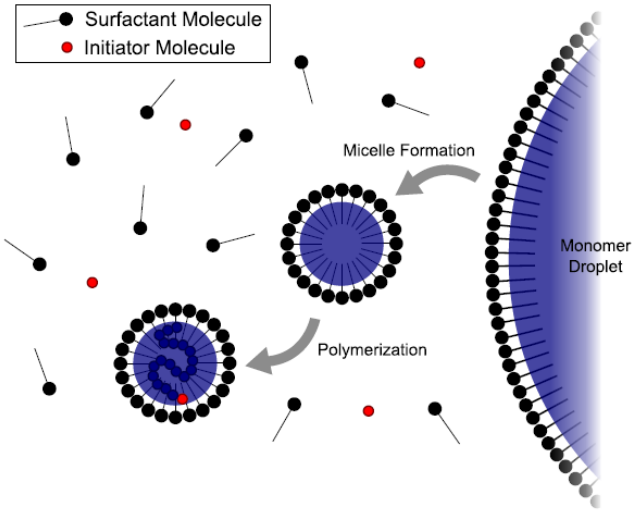

Figure 4. Schematic representation of the emulsion polymerization.

The change in the polymerization rate for the three intervals is sketched in Figure 5. During Interval I the rate of polymerization increases due to the increase of particles number. In Interval II the rate stays constant because of the constant number of particles, while in Interval III the polymerization rate decreases as the monomer concentration in the polymer particles decreases continuously.

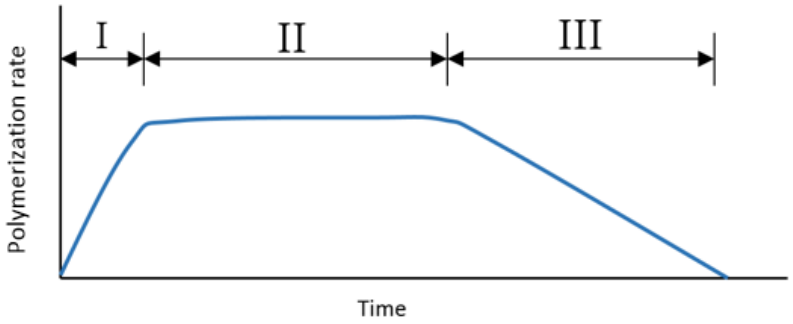

Figure 5. Polymerization rate in the emulsion intervals.

1.5 Glass transition temperature

When the mechanical behavior of the product is a key property, the choice of the monomer is frequently done by taking into account the glass transition temperature, T_g, of the corresponding homopolymer. This temperature is defined with respect to the phase behavior of the polymer as a function of temperature. Starting from molten polymer (T larger than the melting temperature, T_m) and cooling down, solidification starts to take place at T_m while forming different types of polymers:

- Rubbery – under cooling, an amorphous, quite soft polymer is formed; the macromolecules undergo slow translational and conformational reorganization at increasing viscosity (up to 10^{15} poise) aimed to fit into a crystal lattice compatible with the molecular structure (not excessively irregular);
- Glassy – if crystallization does not occur before 10^{15} poise or the molecular structure is too irregular, an amorphous, rigid glass is formed; the temperature at which the rubbery-to-glass transition occurs is called glass transition temperature, T_g;
- Semi-crystalline – if the polymer structure is not too irregular, a partial crystallization is taking place below the melting temperature, being the rest of the material amorphous; very rarely, highly crystalline polymers are formed.

Confining ourselves to fully amorphous polymers, the transition of interest is therefore characterized by the glass transition temperature: a T_g value larger than the operating temperature means that the polymer is glassy at application, while the opposite occurs when the T_g value is lower than the operating temperature. Often for the desired application, a proper mixture of a "hard" monomer (whose homopolymer is characterized by a high T_g) and a "soft" monomer (whose homopolymer is characterized by a low T_g) is used to achieve a copolymer exhibiting the desired value of glass transition temperature. The ratio between the monomers that has to be used to achieve a certain T_g can be evaluated applying the so-called Fox Equation:[2]

$$\frac{1}{T_g} = \frac{\omega_{m_1}}{T_{g_1}} + \frac{\omega_{m_2}}{T_{g_2}} + \cdots + \frac{\omega_{m_n}}{T_{g_n}} \tag{25}$$

where T_g is the glass transition temperature of the final copolymer, T_{g_i} is the one of homopolymer *i*, and ω_{m_i} is the weight fraction of monomer *i* in the final copolymer.
The most commonly used monomers and the T_g values of the corresponding homopolymers are shown in Table 1.[2]

Monomer	T_g of the homopolymer (°C)
1,3-Butadiene	-85
n-Butyl acrylate	-54
2-Ethylhexyl acrylate	-50
Methyl acrylate	10
Methyl methacrylate	105
Styrene	100

Table 1. Glass transition temperatures of homopolymers commonly synthetized by emulsion polymerization.

Many other polymer properties have to be accounted for when choosing the main monomers to be used. In Table 2 possible monomers of choice are summarized as a function of the desired final property.

Desired property	Monomers to be used
Stiffness	Methacrylates, acrylonitrile, stryrene
Soft hand	N-Butyl acrylate, ethyl acrylate, butadiene
Tackiness	2-Ethylhexyl or hexyl acrylate
Water resistance	Hydrophobic monomers like styrene or *n*-butylacrylate
High tensile strength	High T_g monomers like styrene or methyl methacrylate
High elongation	Low T_g monomers like *n*-butyl acrylate or butadiene

Table 2. Desired properties and monomers to be used.

1.6 Spray-drying

The synthesized latices can be used either in the emulsion form or they can be dried to form a powder which can be redispersed in water prior using. In this latter case, the products are defined as redispersible polymer powders (RPPs), which are an example of free-flowing powders. When dispersed in water, they produce again a stable dispersion, whose properties are comparable to the ones of the original latex.[27, 28] They are particularly advantageous in terms of transportation and packaging, they can be handled easier, and they show better storage stability and longer shelf life compared to the liquid product. They are widely used in composite and coating mortars, cement dyes and adhesives, and in the latest years their use has been expanded to drug encapsulation, carrier of functional particles and tile adhesives.[29-32] RPPs require not only a synthesis method that lends the latex a special configuration and specific properties, but also need an appropriate drying technique compatible with the characteristics of the latex particles.[33] The most commonly used technique for drying the RPPs is spray-drying. Thanks to its unique characteristic to preserve the properties of the product during the whole drying process, this industrial operation is worldwide used in many applications, in particular in the products for the food and pharmaceutical industries, such as powder milk, color pigments and active pharmaceutical ingredients (API), which are very delicate.[33, 34]

The spray dryer is a continuous adiabatic drying unit used specifically in processing slurries and solutions, or, more generally, solid particles contained in a liquid phase as fine suspension or aerosol. In particular, it is used in the case in which the product cannot be dried mechanically, when it is sensible to heat, and thus cannot be exposed to high temperature for long periods, or it contains ultrafine particles that can melt and agglomerate during the drying. In the light of the requirements for the product properties conservation,

the most important features of a spray-drying unit are three: i) short residence time in the hot zone of the unit (3-40 seconds). This allows the water film to cover the latex particle until being removed at the end of the process, thus protecting the product from the high temperature. ii) No corrosion issues; iii) control of particles diameter, shape and temperature by tuning the operating conditions.
The drying is carried out at the vaporization temperature, which for an adiabatic process corresponds to the wet-bulb temperature of the heating air. This is defined as the lowest temperature which may be achieved by the evaporation of a water-wetted ventilated surface.

1.6.1 Unit operation

A typical spray-drying unit is sketched in Figure 6.[33]

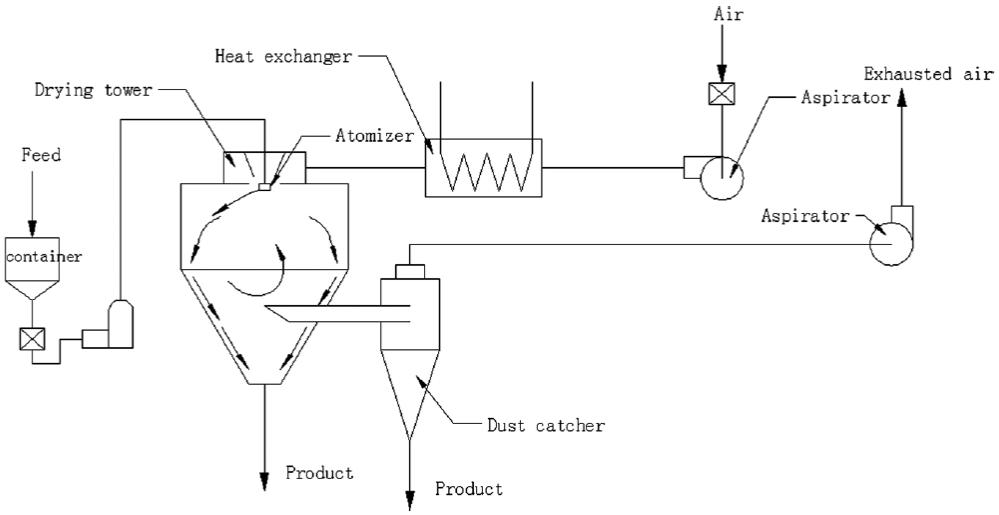

Figure 6. A spray-drying unit.

The core of the technology is represented by the drying chamber, whose design results in a large and tall empty unit, whose size needs to accomplish the following requirements: i) the height must be such to guarantee a sufficient residence time to effectively dry the polymer particles; ii) the internal diameter of the upper part of the chamber has to be wide enough to avoid contact between the wall and the wet droplets.
The drying chamber can be divided in two sections, which mainly differ for shape and temperature. The first section, with cylindrical shape, is characterized by the highest temperature, and represents the part in which the latex particles are dried. The second section, with conical shape, has lower temperature and serves as collector for the dried powder, guiding the particles through the exit. Furthermore, thanks to the particular shape and the reduction of free area for particles motion, this part serves also as first separation

between the gas and the solid particles, by exploiting the contact of the powder with the walls of the unit.

The latex enters continuously inside the drying chamber through an atomizer. This device is a high-pressure nozzle that operates the atomization by forcing the liquid, fed through high pressure pumping, to pass through a tortuous path up to a small orifice with a relevant degree of rotation. It consists of a body with thick walls composed by a stationary helix with a small opening: the liquid crosses the helix assuming a rotating movement and exits from the orifice of the nozzle, diffusing in a cone of small droplets. The atomizer can be installed at different heights inside the unit, however, the installation at the top of the unit allows to better protect the polymer particles from the high temperature. In this way, droplets are fed at the hottest point when they are still covered by the layer of water, and exit dried at the lower temperature, avoiding the powder to be exposed to too high temperatures that may cause a change in the product properties.

In a spray dryer, as well as in many other drying units, heat and mass transfers occur for direct contact between the hot gas (or air) and the dispersed liquid droplets. For this purpose, a flow of air, or gas, is fed inside the unit, together with the latex. As in the case of the atomizer installation, also for the air/gas feed it is possible to choose among three configurations: co-current, counter-current and a combination of the two. Although the counter-current configuration gives higher efficiency thanks to a better heat exchange, co-current configuration is preferred, as it ensures a protection of the droplets from too high temperatures since the very entrance of the latex inside the unit. The major part of the water covering the particles surface evaporates almost instantaneously as the droplets exit the atomizer, due to the high temperature and the presence of the convective flow. The dried particles are then surrounded by air and the remaining water is removed by the gas while the droplets move along the unit.[35] In addition to the drying function, the air flow is also used to avoid the contact of particles with the wall. If particles touch the wall during the drying operation, they stick onto it due to their humidity. If some particles remain attached to the wall, the formation of large agglomerates and grains will be unavoidable and the residence time of their exposure to high temperature increases exponentially. The consequent detachment and precipitation of these agglomerates, known as decanting, would cause a significant change in the product quality. Once the wet air/gas comes out of the drying chamber, some of the smallest particles are dragged together with the air/vapor flux. Therefore, a stage of separation for product recovery and air cleaning is required. This section may include a cyclone separator and other more efficient units, such as bag filters and electrostatic separators.

Some polymer dispersions, and in particular the one made of soft polymers, tend to coalesce during or after spray-drying leading to a coarse powder which is often unwanted for further applications. To prevent that, anti-caking agents like silicon or calcium dioxide can be added. These hard inorganic particles isolate the latex droplets avoiding their possible contact.

Furthermore, thanks to their hydrophilicity, these compounds are also used to help the drying of the liquid solution. In addition, the feedstock can be mixed with additives like polyvinyl alcohol (PvOH) or cellulose which act as protective colloids covering the particles surface and preventing coagulation (as sketched in Figure 7).[33, 36, 37]

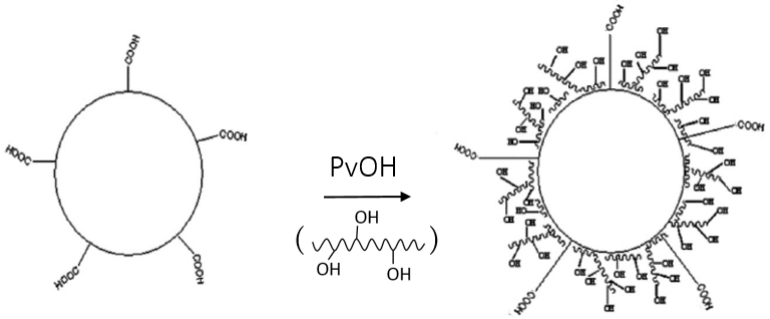

Figure 7. Protective mechanism of PvOH.

1.6.2 Morphology of the dried particles

One of the advantages of spray-dryers with respect to the other drying units adopted for slurries and solutions is the production of almost spherical dry solid particles. However, regardless of the almost spherical shape, the solid particles obtained could have different features, as shown in Figure 8.[38]

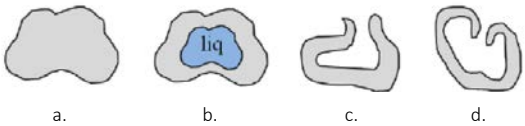

Figure 8. Different morphologies of the solid particles obtained *via* spray-drying.

As Walton *et al.* stressed in their work [39], the parameters affecting the morphology of the dried particles can be numerous and, for this reason, difficult to assess. These include the residence time of the particles inside the drying chamber, the conditions of atomization, the way the air contacts the droplets, the temperature inside the chamber and feed parameters, such as concentration and temperature.

Although each parameter plays an important role, the effect of temperature is believed to be the most significant.[35, 36, 39] According to the study of Chen *et al.*[35] high temperatures (> 175 °C) lead to the formation of cratering grains, while almost spherical grains are obtained at lower temperatures (< 155 °C). A more detailed explanation can be made by considering the Biot number, *Bi*, for the specific particle. This dimensionless number depends on the ratio between the ability of the system to receive heat from outside, which is proportional to the convective heat-transfer coefficient, and the ability of the

system to diffuse the heat internally by conduction, which is proportional to the ratio between the particle thermal conductivity and its diameter:[38]

$$Bi = \frac{hD_p}{k} \tag{26}$$

where h is the heat transfer coefficient, k the thermal conductivity of the solid and D_p the diameter of the particle. According to the value assumed by the *Bi* number, different types of solid granules are obtained at the end of the drying process:

- Case 1: $Bi \ll 1$
  The system presents limited ability in receiving heat, but a very good tendency in distributing it internally. In this case, the drying of the solid particle takes a long time but results as uniform, and so is the particle shape (Figure 8a).

- Case 2: $Bi \gg 1$
  The system presents a strong ability in receiving heat but limited in distributing it internally. Therefore, due to the internal resistance to the heat transfer, the drying occurs only on the particle surface, forming a solid crust characterized by lower material conduction and diffusivity with respect to the liquid. As a consequence, *Bi* increases leading to the formation of an impermeable crust. The liquid trapped inside the crust starts evaporating due to the high temperature, causing an increase of pressure inside the particle. According to the resistance of the crust, three different scenarios may verify: i) if the crust is completely stiff, the droplet explodes due to the high pressure caused by the vapor inside the particle (Figure 8c). ii) If the crust resists to the pressure increase due to the heating, it could implode (Figure 8d). iii) If the crust is sufficiently elastic to resist the volume variations, a solid sphere is formed with the liquid still inside (Figure 8b).

1.6.3 Modeling equations

Spray-drying is a continuous process that involves both heat and mass transfer. The former is due to the supply of heat to the droplets to be dried, which includes the heat supplied through radiation, the convection heat connected to the drying medium and the amount of heat necessary to vaporize the water. The drying process can be modeled, with some approximations, by considering a single droplet moving in a control volume of gas with a given velocity. The droplet of water containing the polymer is considered perfectly spherical and made of a single pseudo-phase of both polymer and water. Steady-state conditions are assumed. With this assumption, it is possible to write the mass and energy balances for the

single particle. These balance equations can be then generalized to the whole set of particles by multiplying the values obtained for the particles density by the total unit volume.[38]

Mass balance

The driving force of the mass transfer is represented by the difference in pressure between the water in the air stream and the one evaporating inside the droplet. In fact, by definition of pressure gradient, the evaporation occurs as long as the partial pressure of the water (P_w), present as moisture in air, is lower than the vapor pressure of the water at the particle temperature ($P°(T_P)$):

$$\Delta P = P°(T_P) - P_w \tag{27}$$

The variation of mass along the axial coordinate *z* is caused by the convective flux entering or leaving the system:

$$\dot{m}_P^{tot}|_z - \dot{m}_P^{tot}|_{z+dz} = J_{CONV}^{tot} dV \tag{28}$$

By substituting the mass flux exiting the system ($\dot{m}_P^{tot}|_{z+dz}$) with its Taylor expansion truncated at the first order, and considering the control volume $dV = Adz$, Equation (28) can be simplified as follows:

$$-d\dot{m}_P^{tot} = J_{CONV}^{tot} A dz \tag{29}$$

where A is the cross sectional area of the drying chamber.
The convective flux per unit volume can be computed as

$$J_{CONV}^{tot} = k_{conv} S_P \Delta P \tag{30}$$

where k_{conv} represents the coefficient for the convective exchange and S_P the particle surface. On the other hand, the differential of the total mass of the particle can be expressed as:

$$d\dot{m}_P^{tot} = v_P A dm_P \tag{31}$$

with v_P velocity of the particle and m_P the mass of the particle.
By substituting Equations (27), (30) and (31) in Equation (29) it is possible to obtain the final equation of the mass balance:

$$v_P \frac{dm_P}{dz} = k_{conv} S_P (P_w - P°(T_P)) \tag{32}$$

Energy balance

In this case, the driving force of the thermal transfer is given by the difference in temperature between the hot gas, which provides the heat for evaporation, and the particle that receives the heat. In fact, by definition of temperature gradient, the heat transfer occurs as long as the temperature of water in the solid (T_P) is lower than the one of the hot gas (T_{hg}):

$$\Delta T = T_{hg} - T_P \tag{33}$$

The variation of enthalpy along the axial coordinate *z* is related to the heat flux due to the evaporation of the liquid phase ($\dot{H}_{ev}$) and the convective thermal flux (J_{TH}^{tot})

$$\dot{H}|_z - \dot{H}|_{z+dz} - \dot{H}_{ev} = -J_{TH}^{tot} dV \tag{34}$$

As in the case of the mass balance, by substituting the enthalpy flux exiting from the system with its Taylor expansion truncated at the first order and considering $dV = Adz$, Equation (34) can be rewritten as follows

$$d\dot{H} + \dot{H}_{ev} = J_{TH}^{tot} A dz \tag{35}$$

The convective thermal flux per unit volume can be expressed as

$$J_{TH}^{tot} = hS_P \Delta T \tag{36}$$

where h is the heat transfer coefficient, and S_P the particle surface. The differential of the enthalpy power ($d\dot{H}$) can be written as

$$d\dot{H} = \dot{m}_P^{tot} dh_{liq}^P(T) + h_{liq}^P(T) d\dot{m}_P^{tot} \tag{37}$$

where h_{liq}^P represents the enthalpy of the liquid phase in the particle. By considering this enthalpy as only function of the temperature, it is possible to write

$$dh_{liq}^P = c_P^L dT \tag{38}$$

Therefore, by obtaining from the mass balance the expression for $d\dot{m}_P^{tot}$ as

$$d\dot{m}_P^{tot} = -k_{conv} S_P \Delta P A dZ \tag{39}$$

it is possible to substitute Equations (38) and (39) in Equation (37), which becomes

$$\dot{m}_P^{tot} c_P^L dT + h_{liq}^P(T) d\dot{m}_P^{tot} - d\dot{m}_P^{tot} h_{vap}^P(T) = hS_P \Delta T A dz \quad (40)$$

Finally, since:

$$h_{liq}^P(T) d\dot{m}_P^{tot} - d\dot{m}_P^{tot} h_{vap}^P(T) = -d\dot{m}_P^{tot} \left(h_{vap}^P(T) - h_{liq}^P(T) \right) = -d\dot{m}_P^{tot} \Delta H_{ev} \quad (41)$$

it is possible to obtain the final version of the energy balance by substituting Equations (31), (39) and (41) in Equation (30), obtaining

$$v_P m_P c_P^L \frac{dT}{dz} = \Delta H_{ev} \left[k_{conv} S_P \left(P_w - P^\circ(T_P) \right) \right] + hS_P (T_{hg} - T_P) \quad (42)$$

1.7 Particles containing carboxylic groups

Particles interpenetration represents one of the main issues connected with the spray-drying operation when working with low-T_g polymer particles.[35] If particles coalesce during the drying operation, it is no longer possible to redisperse the obtained powder and the performance of the material will be very different from the one of the original latex. To prevent interpenetration of the particles and improve latex spray-ability, a functional monomer, such as acrylic acid or methacrylic acid, is often added to the reaction recipe in order to provide additional charges onto the particle surface, limiting in this way particles coalescence. Indeed, thanks to the addition of an acid compound, the surface of the particles is enriched by charged groups, which enhance the electrostatic repulsion among the particles themselves.

These acids are able to polymerize together with the monomers, enabling the addition of carboxyl groups (–COOH) onto the particle surface. Thanks to the introduction of the hydrophilic carboxyl groups, the presence of AA or MAA enhances the polymer performance during the drying phase. However, at the reaction conditions the ionization degree of the carboxyl group is too low to guarantee good redispersibility of the powder. To overcome this limitation, Pei *et al.*[28] suggested to change the pH of the latex before drying by increasing the basicity of the original latex to a pH higher than 9. Indeed, at such high pH value, the carboxyl groups are deprotonated into carboxylic ions $–COO^-$, which are more hydrophilic, and the positive charge of the quaternary ammonium group of the stabilizer is sufficiently shielded to yield a net negative charge on the particle surface. Furthermore, a stronger electrostatic repulsion force acting among the particles is obtained, as well as more negative charges, leading to a more stable reconstituted latex. The addition of AA and MAA, their influence on the film formation, the effect on the compatibility with cement to form a

membrane and the influence on the crack-bridging properties of the membrane are the main goals of this work and will be discussed later on.

1.8 Core-shell particles

Another possible way to avoid interpenetration of the particles and improve latex spray-ability is to prepare core-shell particles, with a hard layer (shell) around a soft core. The soft core has low T_g and gives the polymer film-forming and crack-bridging properties. On the other hand, the hard shell gives the particles an outer surface with higher T_g, thus being more resistant to coalescence during spray-drying. Core-shell morphologies were intensively studied in the literature, as they can improve both the polymer spray-ability and its redispersion, without affecting the film-forming and crack-bridging properties and without the need of adding expensive additives.[40-44]
In this work, a systematic study on the influence of the core-shell morphology on the spray-ability, film-forming characteristics and crack-bridging properties of a polymer with a glass transition temperature (T_g) lower than -20 °C is presented, focusing in particular on the influence of the shell thickness variation.

1.9 Film formation

Film formation defines the process by which a waterborne dispersion of polymeric particles is transformed into a continuous material.[45] The formation of a film from an aqueous dispersion is a complex phenomenon and different theories have been proposed during the years to assess the forces responsible for this process.[45-47] Film formation can be described as a four-step process (Figure 9):[47-51] (1) State I: concentration of the latex dispersion; (2) State II: particles contact, forming a close packing; (3) State III: particles deformation; (4) State IV: film formation. At the beginning, particles in the initial dispersion are stabilized by the surfactant adsorbed on their surfaces. State I is characterized by the evaporation of water at a constant rate. During this phase the concentration of latex particles increases until particles come in contact one with the other and form an ordered structure. When particles come into contact, phase (2) starts and leads to a close packing of non-deformed particles. The closest possible packing of monodisperse spheres corresponds to a water content of approximately 0.35 g water/g polymer.[48] Once the particles are packed in the closest possible way, a significant particles deformation takes place.[52] This phenomenon, referred to as State III, can take place only if drying occurs at a temperature well above the minimum film-forming temperature (MFFT). This temperature is an important characteristic of any polymer emulsion used especially in coatings, where the film

properties are important.[53] In particular, it is defined as the drying temperature above which a transparent and crack-free film is obtained.[48] This temperature is polymer specific and, even though its value is quite close to that of T_g (±10 degrees), it is affected by other properties such as particle size and morphology. Due to the continuous shrinkage that proceeds beyond the point of particles contact, particles deform to fill the volume formerly occupied by water. In order to do so, particles surfaces need to acquire a flat shape, transforming themselves in polyhedra.[54] Then, if the temperature is higher than the glass transition temperature, phase (4) takes place, ending in a homogeneous polymer film. In particular, if the drying temperature is well above the MFFT, particles deformation is sufficiently strong to destroy the hydrophilic network of the surfactant present at the particle-particle interface, forming a non-porous film. On the other hand, if the drying temperature is close to the MFFT, particles deformation is incomplete, and the final film will be characterized by a porous structure of individual particles with hydrophilic surfactant material accumulated in-between the particles.[48, 49]

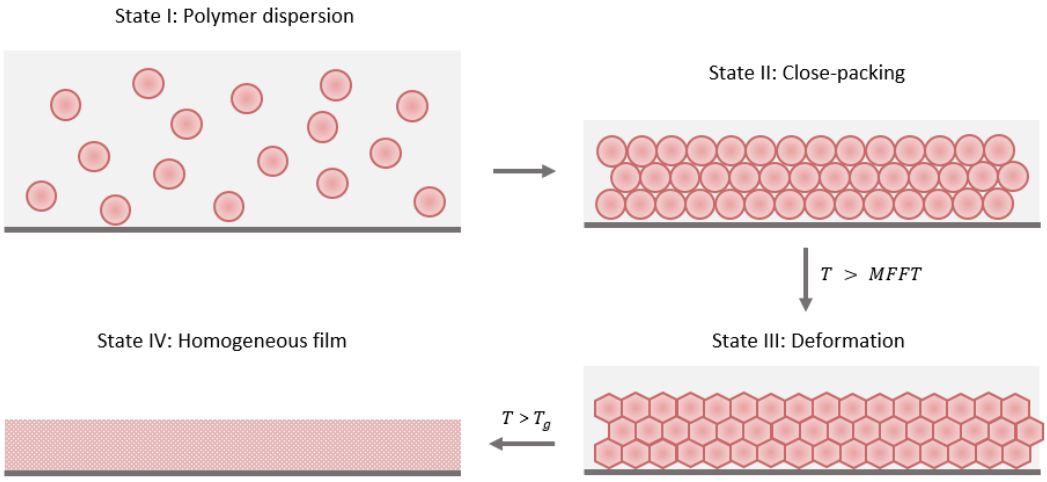

Figure 9. Schematics of the process of film formation.

1.10 Polymers in waterproofing applications

Polymers represent not only versatile materials to be used on their own, but can also be employed in composite materials for construction purposes.[42, 55-59] In particular, the use of polymers as a modifier for mortars and concrete is well-known. Polymer-cement mortars (PCMs), in fact, are prepared by adding polymers to a traditional cement mortar and are widely used as high-performance, low-cost construction materials thanks to their excellent performance and durability.[55, 56, 60] The addition of polymers is known to improve the workability of fresh mortars, the flexibility, the adhesive performance, the water

impermeability and the freezing-thawing resistance of hardened mortars.[57, 58, 61] Especially, crack-bridging and waterproofing properties are of major interest for the construction industry. In particular, crack-bridging properties are ensured by the improved adhesion of the mortar constituents of PCMs among themselves and a higher chemical resistance due to the presence of polymer films which reinforce the membrane network (Figure 10).[55] Furthermore, polymer-cement mortars provide a cheap and green alternative to other waterproofing methods, like for example bituminous sheet-based systems, which arrive at the construction site as rolls and are then laid on the surface, thus requiring substantial work as the resulting joints need to be carefully sealed as they represent a potential weak spots. In addition, under an economic point of view, the higher initial price of the latex-modified systems are compensated by the reduced maintenance costs and the increased service life guaranteed by the excellent durability characteristics of the PCMs.[57] Polymer-cement mortars systems for waterproofing can be divided into two categories, one-component (1C) and two-component systems (2C).[27, 62] In 2C systems, the polymer is present in the form of a latex dispersion that needs to be mixed with sand, cement, and water in the right ratio and can then be applied on the supporting structure. These systems, however, are susceptible to human errors during mixing and transport to the construction site is expensive as the polymer comes dispersed in water. 1C systems, on the other hand, come as dry-mixed powder consisting of sand, cement, polymer, and further additives which only needs to be mixed with water on-site. These 1C systems reduce transportation costs, have a longer shelf life and are easy to use.[63] In order to be suitable for the use in a 1C system, a polymer needs to have several properties, some of which contradict others. The synthesis of such polymer must be easy and effective, also the price of the ingredients should be as low as possible. It needs to have a low T_g and be film-forming, to provide a waterproof, flexible and crack-bridging membrane in an appropriate temperature range. Furthermore, the dispersion needs to be spray-dried, which contradicts the low T_g, as a soft polymer facilitates caking during spray drying. To provide a powder usable with cement, it has to be compatible upon mixing with the cement without leading to quick coagulation and without forming a two-phase system. Also, the polymer powder needs to be redispersible in water without losing its properties.

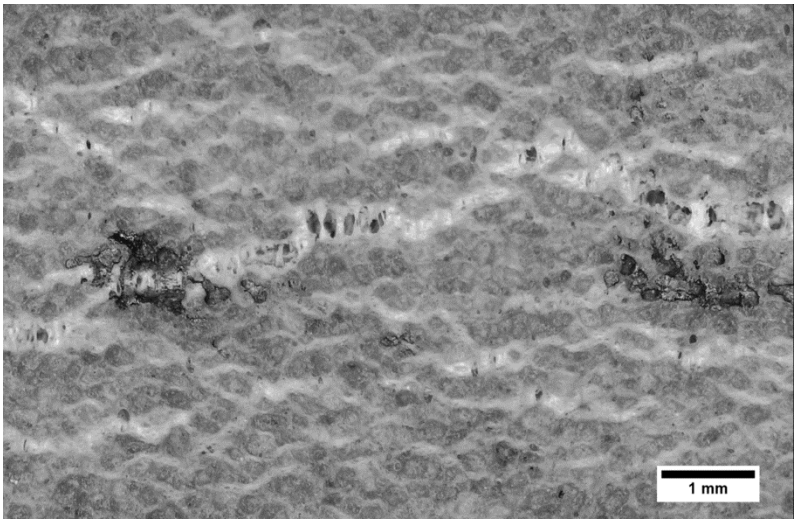

Figure 10. Crack-bridging action of the polymer film in a membrane subjected to tensile strain.

2. Aim of the thesis

This project aims to synthesize a latex, *via* free-radical emulsion polymerization, characterized by high solid content and glass transition temperature lower than -15 °C. The produced polymer dispersion must be film-forming, spray-dryable, and the obtained powder has to be water redispersible. In particular, for optimal spray-drying performances, the nanoparticles have to be larger than 300 nm. Moreover, the obtained dried powders have to be compatible with the cementitious mortars and need to form a uniform membrane exhibiting good crack-bridging and waterproofing properties, when tested at different temperatures. To guarantee particles stability and avoid coagulation during spray-drying, two different particle structures are investigated. The first includes the addition of positive carboxyl groups onto the particle surface, which leads to an increased repulsion between the particles, thus limiting their interpenetration. In the second system, core-shell geometries made of a hard shell onto a softer core are presented. In this case, when particles come in contact, the coagulation is limited by the presence of the hard surface. In particular, the effect of different types and percentages of acids as well as of the different core-shell geometries on the spray-drying operation is systematically explored.

3. Experimental

3.1 Materials

For the syntheses styrene (STY, 99.5% stab. with 10-15 ppm 4-t-butylcatechol from ABCR), 2-ethylhexyl acrylate (2-EHA, 98% from ABCR), methyl methacrylate (MMA, 99% stab. with MEHQ from Sigma-Aldrich), acrylic acid (AA, 99.5% stab. with 200 ppm 4-methoxyphenol from Alpha Aesar), methacrylic acid (MAA, 99.5% stab. With 250 ppm MEHQ from Acros Organics), have been used as monomers, 2,2'-Azobis (2 methylpropionamidine) dihydrochloride (V-50, 98% from Acros Organics) as initiator, [3-(Methacryloylamino)propyl] trimethylammonium chloride solution (MAPTAC, 50 wt.% in H_2O, from Sigma-Aldrich) as stabilizer. All materials were used without further purification. Deoxygenated Millipore water (Merck Millipore Synergy) was the reaction medium for all syntheses. To change the pH of the latex, sodium hydroxide 1 M and hydrochloric acid 0.1 M were used. For spray-drying fumed silica, dolomite, and polyvinyl alcohol (Höppler viscosity 4 mPa·s, hydrolysis degree 88 mol%) were used as received. Chloroform-d (99.8 atom%D, stab. with Ag, Armar Isotopes) was used for NMR characterization as is. For cement compatibility and crack-bridging tests, Portland cement (CEM I 52.5N Milke classic, Milke) and quartz sand (0.1 - 0.3 mm) were used.

3.2 Syntheses

The semi-batch emulsion polymerization was carried out in a 1 L glass jacketed reactor fitted with a reflux condenser, sampling device, N_2 inlet, two feeding inlets and a PTFE anchor stirrer equipped with two blade impellers rotating at 200 rpm. For the polymerization, the reactor (Syrris Atlas automated reaction system) was charged with a solution (IC) of MAPTAC in deionized water or with deionized water only, depending on the specific synthesis. The water was deoxygenized by bubbling it overnight with N_2. The reactor was heated up to 80 °C using the heating jacket connected to the oil bath (Huber polystat CC 302) and, after reaching the reaction temperature (± 0.5 °C), part of the initiator solution (IS) was added into the reactor as a shot. According to the type of particles to synthesize, different ingredients and feeding methodologies were chosen.

3.2.1 Synthesis of polymer particles with the addition of carboxylic groups

According to the choice of the co-monomer to be fed together with 2-EHA, the charge at the beginning of the reaction might be represented by the mixture MAPTAC-deionized water or by deionized water only. In the case of the use of styrene as co-monomer, after addition of the initial shot (IS), the remaining initiator solution (IF) and monomer mixture (CF) were fed using two Bischoff HPLC compact pumps. The initiator was fed for 6 hours and the monomer mixture containing STY/2-EHA for 2h. In order to avoid secondary nucleation or the formation of too small particles, the mixture of STY/2-EHA with the addition of a certain percentage of AA or MAA was fed for 2h, after the completion of the previous monomer feed and 1h rest, when the cumulative conversion reached a value of approximately 80%. After switching off the initiator feed at 6 hours, the reaction was stirred for an additional hour to ensure full conversion. Conversely, when MMA was used, only deionized water was charged in the reactor, and the mixture MAPTAC-deionized water was fed in time using a Hitachi HPLC pump for 5h. In this case, different feeding combination, timing and reactor temperature were investigated, keeping the percentage of AA constant and equal to 1%, which resulted in best performances. Differently from the case with styrene, no rest time was needed in the case of two different feeds due to the higher reactivity of MMA, giving high conversion since the very first hours. The detailed reaction formulations are reported in the discussion section in Tables A1 and A2.

3.2.2 Synthesis of core-shell polymer particles

Once the initial solution of MAPTAC in deionized water, or deionized water only, inside the reactor reached a temperature of 80 °C, after addition of the initial shot (IS), the remaining initiator solution (IF) and monomer mixture (CF) were fed using two Bischoff HPLC compact pumps. The initiator was fed for 6 hours, the core monomer mixture was fed for 3 to 4 hours depending on the core-shell ratio used. After switching off the core feed, it was waited for 1 to 1.5 hours (WT) until the conversion reached approximately 80%. The shell feed (SF) was then switched on for 0.5 to 1.5 hours. After switching off the initiator feed, the reaction was stirred for an additional hour to ensure full conversion. Depending on the type of monomer mixture used and on the desired particle size, a different feeding method for the MAPTAC-deionized water solution was applied. Indeed, in the case of STY/2-EHA solution, the stabilizer-water solution was charged at the beginning of the reaction, without further addition during the reaction time. However, due to the small particle size obtained by charging all the stabilizer at the beginning, in some cases the amount of initial surfactant has been lowered, and part of the stabilizer solution was fed in time using a Hitachi HPLC pump for 3 to 5.5 hours. For the system MMA/2-EHA, the entire surfactant solution was fed in time using a Hitachi HPLC pump for 5 to 5.5 hours. In the case in which carboxyl groups were

added to the particles surface, 1% of acrylic acid was introduced in the shell mixture, maintaining the synthesis procedure equal to the one described above. The detailed reaction formulations are reported in the discussion section in Tables A3 and A4.

3.3 Product characterization

The produced materials are characterized during the reaction in terms of particle size, instantaneous conversion and composition. To do so, a sample was taken hourly from the polymerization reactor. Once the final product was obtained, the glass transition temperature of the polymer, the pH, and the surface zeta potential of the latex were evaluated. For the complete characterization of the products, the following techniques have been adopted.

3.3.1 Dynamic light scattering

Dynamic light scattering (DLS) is a non-destructive technique widely used for measuring the size and the size distribution of nanoparticles in liquids.[64] In particular, it utilizes the illumination of a particles suspension undergoing Brownian motion by a laser beam and evaluates the light scattered back by the particle into the laser cavity. Given the same temperature and viscosity conditions, small particles move quickly, creating rapid variations of the scattering intensity, while large particles move slowly, creating slower intensity variations.[65, 66] Thanks to an auto-correlator, the speed of the intensity variations is measured and the particle diffusion coefficient can be calculated by the correlation function. Thanks to the Stokes-Einstein equation (Equation 43), it is then possible to obtain the particle radius from the inverse formula of the diffusion coefficient:[67, 68]

$$D = \frac{k_B T}{6\pi\mu r} \tag{43}$$

where k_B is the Boltzmann constant, μ is the viscosity of the medium and r is the particle radius. The average radius and the polydispersity index (PDI) of the particle size distribution were measured by a Malvern Instruments ZEN3600 Nanosizer after diluting the sample with deionized water.

3.3.2 Gravimetric analysis

Gravimetric analysis was used to evaluate the moisture content of the latices. The measurements were performed using a Mettler-Toledo HG53 Halogen Moisture Analyzer,

by weighing *ca.* 1 g of product on an aluminum disposable plate previously filled with sand. While heating the sample through a halogen radiator up to 120 °C, the instrument continuously records the sample weight. When the sample no longer loses weight, the measurement is complete and the moisture content is calculated. The total weight loss is used to calculate the solid content, from which the instantaneous conversion of the ongoing reaction is evaluated given the reaction recipe.

3.3.3 ζ Potential

ζ potential is a measure of the magnitude of the electrostatic or charge repulsion/attraction between particles and it is an indication of the system stability.[69] In particular, it gives a measure of the charge distribution on the surface of the polymer and, therefore, provides information on the particle colloidal behavior.[70] After the reaction end, the ζ potential of a 0.01 wt.% solution of the resulting latex was measured using the Malvern Instruments ZEN3600 Nanosizer at 25 °C. When tests at different pH conditions were necessary, 20µL of HCl 0.1M were added to the diluted sample in order to obtain values of pH ≤ 4, while, to obtain pH ≥ 11, 50µL of NaOH 1M were added. Values of ζ potential in the interval 0 - ±20 mV were considered as an indication of unstable particles. A positive value of the measured potential means that the positive charges deriving from the initiator and from the MAPTAC are exposed onto the surface, while a negative value corresponds to negative charges exposed, deriving from the incorporation of AA or MAA, when they were employed.

3.3.4 Nuclear magnetic resonance

Nuclear magnetic resonance spectroscopy, most commonly known as NMR spectroscopy, is an analytical technique that exploits the magnetic properties of certain atomic nuclei. It determines the chemical and physical properties of atoms of the molecules in which they are contained. It is based on the phenomenon of nuclear magnetic resonance and can provide detailed information about the structure, reaction state and chemical environment of molecules. The resonance frequency is altered by the intramolecular magnetic field around an atom, thus giving access to details of the electronic structure of a molecule. NMR measures the nuclear spin resonance, *i.e.,* the relaxation response of nuclei spins upon the application of a magnetic field.[70, 71] The technique that has been applied is known as ^{1}H-NMR, since it measures only the spin resonance for the hydrogen atoms. The time for spin resonance, *i.e.,* the time that a spin takes to come back to its initial state, is influenced by the surrounding environment of each H-atom. To analyze the instantaneous composition of the formed polymer chains, the samples were dried in a vacuum oven at 50 °C and dissolved in 3 mL of deuterated chloroform to perform ^{1}H-NMR experiments using a BRUKER 300 MHz Spectrometer. The evaluation of NMR spectra is explained in Section B.2 of the Appendix.

3.3.5 Differential scanning calorimeter

The glass transition temperature was measured using a Q1000 differential scanning calorimeter (DSC) from TA Instruments. About 10 mg of latex were dried overnight in a vacuum oven at 50 °C in a 40 µL aluminum crucible before starting the measurement. The sample was subjected to heating and cooling rates of 5 °C min^{-1} in a nitrogen atmosphere in the temperature range from -80 to +100 °C, while measuring the heat flow required. The T_g was obtained from the DSC plot by taking the inflection point of the S-shape profile heat flow *vs*. temperature profile, as shown in the Appendix (Section B.1).

3.3.6 Scanning electron microscopy

Scanning electron microscopy (SEM) is a microscopy technique in which a sample is scanned with a focused high-energy beam of electrons to produce an image. The latter is a result of the interaction of the electrons with the specimen and, depending on the angle of the beam hitting the surface, this technique enables to gather information about the surface topography, composition and size of powders. This technique was used to observe powder particles possible aggregation and their structure. SEM images were taken using a Gemini 1530 FEG from Zeiss with field emission gun operated at 5 kV using a Pt/Pd 4nm-thick coating. An example of image obtained using SEM technique is shown in Figure 11.

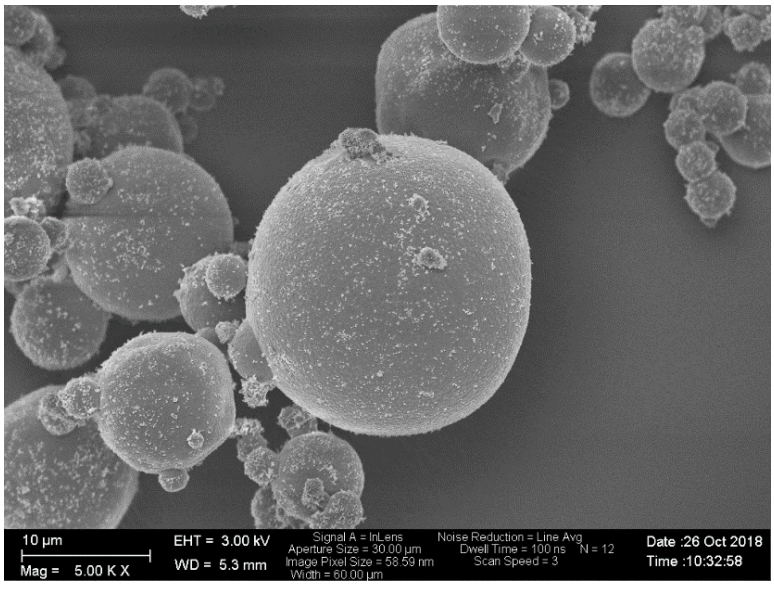

Figure 11. SEM image of sample *Mb*.

3.4 Product processing

3.4.1 Spray-drying

Prior the spray-drying, the latices were tested again for particle size and PDI to ensure no aggregation during storage. For spray-drying in a NiroAtomizer, depending on the type of latex processed, 12% or 15% of polyvinyl alcohol with respect to the polymer was added as protective colloid, and the dispersion was diluted with water to have a total solid content of 25%. The inlet temperature of the spray-drier was kept at 135 °C and the outlet temperature at approximately 70 °C. The compressed air inlet to disperse the anti-caking mixture was set to 2 bar and the spray nozzle was set to 3.5 bar. A peristaltic pump (IKA ISM 817) was used to feed the dispersion at 12.2 g min^{-1}. To prevent caking of the dried powder, silica was fed together with dolomite with a ratio of 1:18 from a dry powder feeder (AccuRate) with a feed rate of 0.75 g min^{-1} to ensure 19 wt.% with respect to the polymer. After the dispersion was fed, the spray-dryer was opened and cleaned using a brush to collect also the powder sticking to the walls. 0.5 g of the resulting powder was taken and mixed with 10 mL of water to test the redispersibility and investigate whether the powder coagulates when put in water.

3.4.2 Polymer-cement compatibility

To test the suitability of the polymer for waterproofing membranes, 25 g of it were dry-mixed with 56 g of quartz sand and 19 g of Portland cement. The dry mix was poured into 19 g of water and a timer was started. It was then stirred vigorously for 1 minute and the wetting speed as well as the amount of water needed were analyzed. If the amount of water was not sufficient to yield a creamy consistency, additional water was added. The polymer-cement mixture was then applied on a plastic foil with a thickness of 2 mm. After 24 hours, the membrane was peeled off and the peeling and bending behavior as well as the surface morphology were analyzed.

3.4.3 Crack-bridging

Crack-bridging tests were performed in the temperature range from -20 to +23 °C at AkzoNobel (see Section B.3), using a Z020/TH2S by Zwick/Roell. The test is a uniaxial tensile test applying a constant displacement rate of 0.15 mm min^{-1}. Before the test and the recording starts, a pre-load of 20N is applied. If the testing temperature deviates from room temperature, the instrument is encased by a temperature controlling unit TEE 65/40X by RS-Simulatoren. A sketch of the sample preparation procedure is shown in Section B.3.

4. Results and Discussion

4.1 Polymer particles with AA/MAA as co-monomer

4.1.1 Synthesis

Polymer particles with carboxyl groups on the surface were produced through the addition of acrylic (AA) or methacrylic (MAA) acid to the reaction formulation, always using styrene or methyl methacrylate as main monomers. The values of final particle size, PDI, solid content, pH, ζ potential and glass transition temperature for all the syntheses with STY/2-EHA at increasing percentages of acid are reported in Table 3 and Table 4. The values of the same final properties are shown in Table 5 for all the syntheses with MMA/2-EHA and 1% AA at different operating conditions. In this case, only 1% of acrylic acid was examined since, from the studies with styrene, it was found to be the best choice, as it will be shown later on. As far as the syntheses with STY/2-EHA are concerned, the particle diameters are in a range between 285 and 304 nm and the corresponding size distributions show low PDI values. Conversely, in the case of MMA/2-EHA and 1% AA, size measurements are in a range between 204 and 413 nm and the distributions show higher PDI values, meaning that the system is characterized by a broader particle size distribution. The presence of particles with significantly different sizes can be explained by considering the phenomenon of secondary nucleation. As a matter of fact, the water-soluble, acid monomer fed into the system is creating new polymer particles, rather than swelling and growing the already existing ones. This fact can be attributed to the larger reactivity and concentration of methyl methacrylate with respect to the co-monomer, which leads to high instantaneous conversion of the first component since the very beginning, while making it difficult for the acid to be incorporated in the polymer. Indeed, as the solubility of AA is much higher in water than in the polymer, it tends to remain in water, thus nucleating new particles very rich in this monomer. In order to favor the copolymerization of the acidic monomer, AA was fed from the very beginning together with the monomer mixture, however a high PDI value was still obtained. This can be again attributed to the higher reactivity of methyl methacrylate, which leads to high conversion since the very first hours. For this reason, as the monomer is fast consumed to form polymer, AA has less time to diffuse into the polymer particles and to be incorporated in the polymer.

During the reaction, the values of particle size and instantaneous conversion were monitored. As expected, in the case of the syntheses involving styrene, both the particle size and the conversion exhibited a rapid increase at the beginning, which got slower at about 5 hours reaction time due to the progressive monomer depletion. In particular, the

instantaneous conversion plot shows the typical S-shape trend. The curves have a similar shape for all reactions, a typical example is shown in Figure 12.

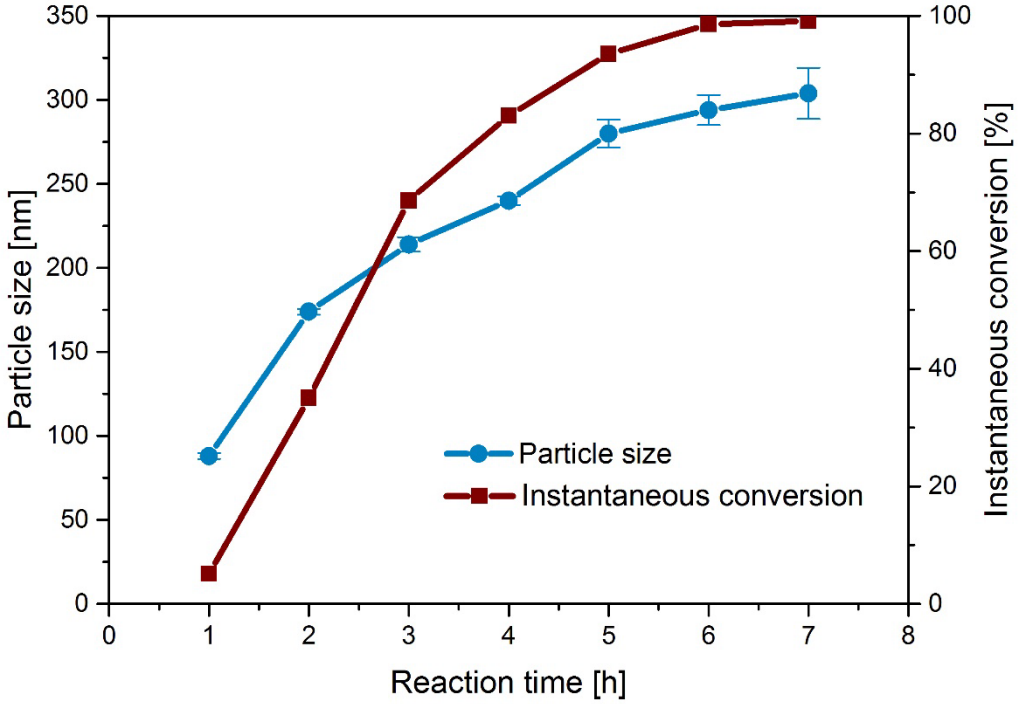

Figure 12. Particle size and instantaneous conversion in time of sample *S3*.

When methyl methacrylate was used, instead, the instantaneous conversion showed a flatter profile at values very close to 100% because of the higher reactivity of this monomer, as it can be seen in Figure 13. The presence of secondary nucleation leads to a system characterized by the presence of both small and large particles. In these conditions, the DLS instrument provides a single value of the average diameter representative of the entire distribution and high values of the polydispersity index. Therefore, the average values of the particle size are not fully representative of the actual distribution and the slowly decreasing trend in the figure could well-be the result of the growth of the larger particles along with the continuous formation of smaller particles.

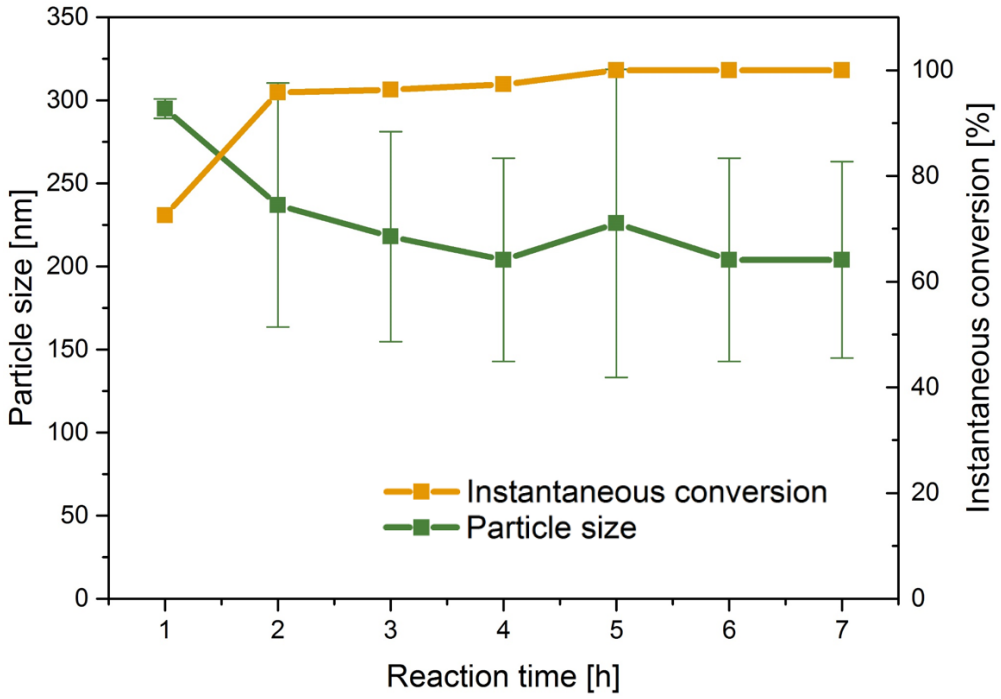

Figure 13. Instantaneous conversion of sample *MI5*.

To monitor the particle composition during the reaction, NMR measurements were performed with the samples taken hourly. By evaluating the integrals of the spectra it was possible to calculate the mass fraction of 2-EHA in each sample. Full NMR results and evaluations are reported in Section C.1. As shown in Figure 14, after a certain time the composition of the copolymer stabilizes around its final value. This value is similar for all samples and, according to the recipe, it should be equal to 0.65 mass fraction (a mixture at 35/65 of STY/2-EHA was used in these cases). The NMR measurements carried out during the first 3 hours of the synthesis are not accurate as it was not possible to distinguish the peaks of MAPTAC from those of 2-EHA. Indeed, as MAPTAC is completely fed at the beginning whereas 2-EHA is fed in time during the reaction, the contribution to the peak intensity of the reactive stabilizer is not negligible and prevents a reliable measurement of the copolymer composition during the first reaction hours.

When the synthesis was complete, final characterization of each sample was performed. DSC measurements were taken in order to estimate the T_g of all the samples. The surface zeta potential, which gives an indication of the surface charge of the particles, was also measured. Since the resulting electrostatic repulsion forces contribute to a stable dispersion and a good spray-ability in the drying step, this value is quite relevant. Due to the presence of both positive and negative charges in the system, the former given by the presence of MAPTAC, the latter by the acrylic/methacrylic acid, the zeta potential was measured at different pH conditions. Indeed, at high pH values, the carboxylic groups deriving from the acid are deprotonated and result in a net negative charge. As shown in Table 3 and Table 4

by increasing the percentage of acid, the values of the ζ potential progressively decrease at all pH conditions. In particular, in the case of samples *SII, SIII* and *S3* at neutral pH, a value of zeta potential lower than 20 mV can be observed, which means that particles exhibit limited stability at this pH condition, which may lead to aggregation during storage as dispersion or to coagulation when subjected to the high shear force during spray-drying. In the case of samples synthesized with methacrylic acid, instead, sample *MI3* shows low stability at neutral condition, while samples *MI2* and *MI4* lack stability at basic pH, indicating that the acrylic acid was almost fully incorporated inside the polymer particle and not at its surface. In general, positive values of ζ potential means that the positive charges deriving from MAPTAC are exposed on the surface, while negative values correspond to the negative charges exposed, deriving from the presence of the carboxylic groups of the acid. The loss of stability due to change in pH can be explained with the change in exposed charges onto the surface. The synthesized latices are characterized by acidic pH and by the presence of mostly positive charges onto the particles surfaces. The addition of water, necessary for the dilution of the products, neutralizes the pH and the negative charges belonging to the acid start to be exposed on the surface together with the positive ones. If the negative charges are enough to counteract the contribution of the positive ones, the particles have a net limited superficial charge. Without any type of repulsion, neither electric nor steric, particles dispersion may aggregate already during storage and even more when subjected to high shear force, as in the case of spray-drying operation explained later on.

To make sure the synthesized latex is usable for a waterproofing membrane, the ability to form a film has been tested. All latices resulted film-forming after synthesis, used as is.

Sample name	*S*	*SI*	*SII*	*SIII*
AA	0%	1%	3%	5%
Size [nm]	285	284	288	301
PDI [-]	0.01	0.02	0.04	0.02
Solid content [%]	39.07	40.40	39.23	41.26
pH [-]	6.5	4.5	4	3.5
ζ potential [mV] – pH 4	54	57.7	40.3	37.3
ζ potential [mV] – pH 6-7	51	29.2	18.4	4.94
ζ potential [mV] – pH 11	47.8	-44.3	-39.8	-39.3
T_g [°C]	-13.56	-14.25	-20.39	-29.78

Table 3. Final particle size, PDI, solid content, pH, ζ potentials and T_g of the latices STY/2-EHA with different acrylic acid percentages.

Sample name	*S1*	*S2*	*S3*
MAA	1%	3%	5%
Size [nm]	294	288	304
PDI [-]	0.05	0.03	0.05
Solid content [%]	40.77	39.24	40.32
pH [-]	5	4.5	4.5
ζ potential [mV] – pH 4	60.1	25.7	45.7
ζ potential [mV] – pH 6-7	31.1	51	0.8
ζ potential [mV] – pH 11	-35.3	-42.4	-41
T_g [°C]	-17.1	-21.45	-24.98

Table 4. Final particle size, PDI, solid content, pH, ζ potentials and T_g of the latices STY/2-EHA with different methacrylic acid percentages.

Sample name	*MI1*	*MI2*	*MI3*	*MI4*	*MI5*
Size [nm]	413	430	214	384	204
PDI [-]	0.2	0.2	0.4	0.3	0.3
Solid content [%]	38.19	38.73	39.06	39.14	39.17
pH [-]	5	5	5	5	5
ζ potential [mV] – pH 4	52.2	50.3	56.2	54.4	48.4
ζ potential [mV] – pH 6-7	47.8	28.6	16.6	45.2	41.4
ζ potential [mV] – pH 11	-27.8	-7.2	-26.5	-2.11	-21.9
T_g [°C]	-24.05	-23.75	-23.98	-21.18	-19.30

Table 5. Final particle size, PDI, solid content, pH, ζ potentials and T_g of the latices MMA/2-EHA with 1% AA at different operating conditions.

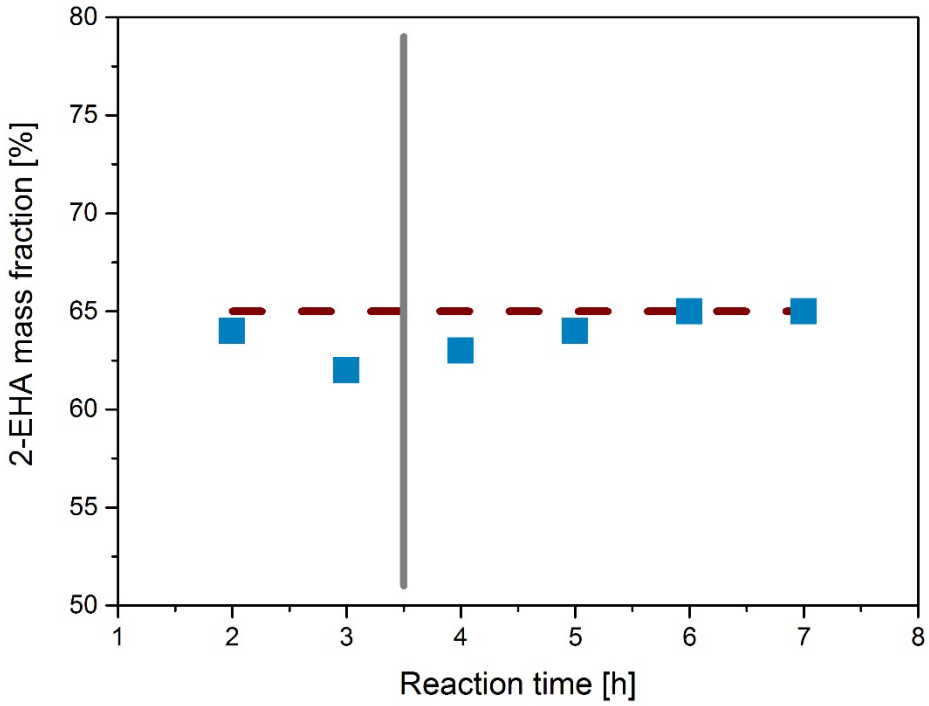

Figure 14. Mass fraction of 2-EHA in the polymer particle for the sample *SIII* during the reaction. The dashed curve represents the cumulative polymer composition corresponding to the fed monomer mixture assuming complete conversion. NMR results start to be reliable from the grey line on.

4.1.2 Spray-drying and redispersibility

All latices were stable and did not show aggregation before being processed into the spray-drier. Trials were conducted to find the right parameters values to be used for optimal drying operation. In particular, the amount of PvOH was observed to have a relevant influence on the resulting dried powder. It is important to highlight that the operating parameters are unit-dependent and different spray-towers may show different results. In this case, all samples could be sprayed with an amount of PvOH of 12% with respect to the polymer and dry powders were obtained. Spray-drying operation was considered successful when a free-flowing, fine-grained sized powder was obtained and, in particular, if the free-flowing ability after 24 hours of storage was preserved (*i.e.*, non-caking systems).

The latex obtained after the synthesis with AA/MAA is acidic (pH in the range 3.5-5). As previously reported, the charges exposed on the surface of the particles and therefore their stability, highly depend on the pH of the latex. As it can be easily understood, this will also affect the performance during spray-drying. It is therefore important to investigate which pH conditions lead to best spray-ability and optimal crack-bridging properties.

During sample preparation before spray-drying, the pH of the latex becomes neutral due to the addition of PvOH and the dilution with water to a solid content of 25%. At these

conditions, spray-drying of the latex was not possible, due to the clogging of the nozzle in the very first minutes. This is due to the limited stability of the particles at neutral pH, as reported in Table 3 and Table 4.

In order to test the spray-ability at basic conditions, the pH value of the original emulsion was adjusted to about 9-10 using a 1 M solution of sodium hydroxide. This adjustment of pH of the latex is necessary for three main reasons: i) some of the samples show a value of zeta potential between +20 and -20 at neutral pH, meaning that the particles show limited stability at this pH condition and may coagulate when subjected to the high shear force present in the spray-dryer nozzle; ii) by deprotonating the carboxyl groups –COOH into –COO^-, a more hydrophilic species is obtained, improving the redispersibility of the powder; iii) –COOH groups are very reactive and latex particles easily react with each other forming –$COOCO^-$ groups, if the pH is lower than 9.[28] Thus, aggregation of latex particles is very likely, making redispersion of the powder more difficult. Furthermore, –$COOCO^-$ groups are less hydrophilic than carboxyl groups and their presence reduces the redispersibility of the powder. Latices processed at basic pH values after the addition of 12% PvOH resulted in fine-grained sized powders, with free-flowing characteristics after 24 hours.

To investigate the spray-drying at acidic pH values (pH < 4), a solution of 0.1 M HCl was added dropwise to the latex. Also in this case, fine-grained sized powders were obtained. However, redispersibility and crack-bridging properties were worse with respect to the powders obtained by changing the pH to basic conditions, for the reasons described above. The same behavior has been also reported by Pei *et al.* [28]

Spray-drying with a lower amount of PvOH (< 12%) was not successful in our unit. However, when the same operation was performed by the industrial partner using a 5 meter-tall tower, a lower amount of protective colloid could be used (9%). This means that it is possible to reduce the amount of needed PvOH using a larger spray-drying unit while ensuring the same product quality. This fact can be attributed to the longer residence time in a taller tower, which can dry the particles at larger extent, thus limiting their stickiness.

Images obtained by SEM show that the sample containing methyl methacrylate gave finer powders with respect to the samples synthesized with styrene. This can be attributed to the larger size characterizing all the particles prepared with MMA with respect to the ones with STY. Indeed, the larger the particles, the lower is the possibility of agglomeration when sprayed inside the chamber at constant amount of protective colloid, as lower area is exposed.[46]

Redispersibility was measured to analyze the behavior of the dried polymer powders when mixed again with water. In principle, it was possible to redisperse all samples by simple stirring and none of them formed immediately large pieces of coagulated polymer. The redispersibility was visually assessed and the results are shown in Table 6. These results show that a good spray-ability does not necessarily mean that the dried powder is well-redispersible.

In general, a better method would be desirable to properly quantify redispersibility. Several trials using a centrifuge failed, as the colloids were too heavy to stay in solution even at low rotation rates for short times. A possible solution would be to measure the UV absorbance, but this would require a precise calibration.

Sample name	S_I	S_{II}		S_{III}	S_1	S_2	S_3	M_{I1}
pH condition	Basic	Acid	Basic	Basic	Basic	Basic	Basic	Basic
Redispersibility	gr	mr	mr	br	gr	gr	gr	vgr

Table 6. Results of the visual analysis of the redispersed polymer powder with styrene as co-monomer. Assessment ranges from very good (vgr) over good (gr), to medium (mr) and bad redispersibility (br).

Again, with reference to Table 6, good to medium redispersibility has been obtained for all the samples, except for those containing 5% AA. Redispersibility of powder obtained from the synthesis with methyl methacrylate and 1% AA was very good, with very small aggregates present in the redispersed solution. This improved behavior with respect to redispersibility can be attributed to the higher hydrophilicity of methyl methacrylate with respect to styrene.

4.1.3 Crack-bridging and polymer-cement compatibility

Results of the expansion-by-crack test for samples containing STY/2-EHA and different percentages of acrylic acid are shown in Figure 15. Compared to the base membrane, made using powder consisting only of STY/2-EHA, the membranes formed by latices containing acrylic acid show always a better crack resistance, particularly at room temperature where the perfomrance are significantly higher. However, it is not possible to see a well defined trend with respect to the acid percentage as all the membranes behave almost identically at low temperatures. As expected, the performance of all samples decreases at low temperatures, as the polymer becomes harder and more brittle. A more significant comparison can be made looking at Figure 16. As already noticed, when spray-dried both in acidic and in basic conditions the samples synthesized with acrylic acid show improved crack resistance with respect to the base membrane. In particular, the sample with 3% AA (S_{II}) sprayed in basic pH conditions shows the largest possible expansions at every temperature, with respect to the same sample sprayed in acid pH condition and to the sample with 3% MAA (S_2). However, in the case of the sample containing methacrylic acid, the presence of this acid doesn't have a positive effect on the crack-bridging properties, and the obtained membrane shows the worst behaviour, even with respect to the base membrane.

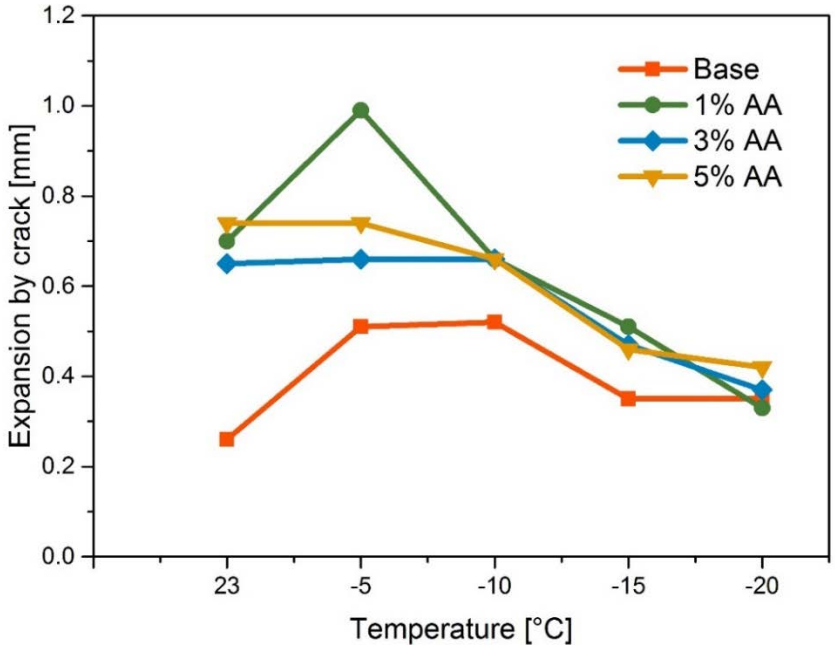

Figure 15. Expansion in millimeters before the membrane breaks at different temperatures for STY/2-EHA with different AA percentages.

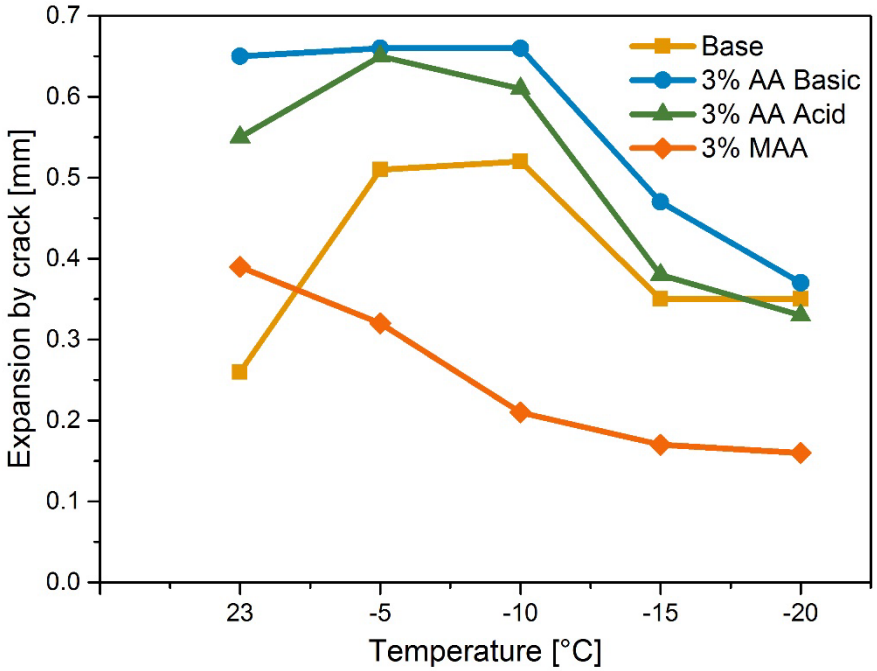

Figure 16. Expansion in millimeters before the membrane breaks at different temperatures for STY/2-EHA + 3% AA or MAA samples.

As far as samples with MMA/2-EHA and 1% AA are concerned, although the addition of the acid enhances the crack resistance with respect to the base case (represented by a

membrane obtained from a powder containing only MMA/2-EHA), the performances are worse with respect to the sample constituted by STY/2-EHA and 1% AA (Figure 17).

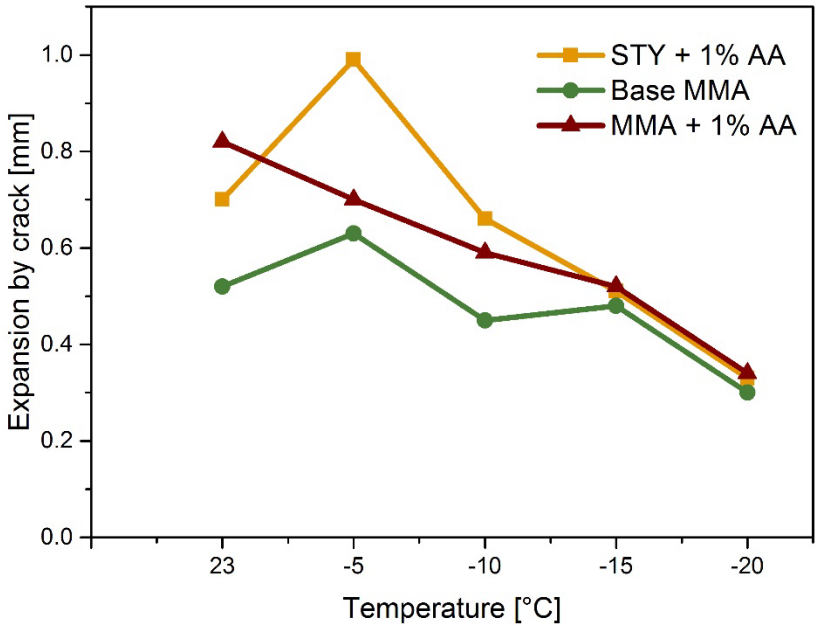

Figure 17. Comparison of the expansion in millimeters before the membrane forms cracks at different temperatures of samples with STY/2-EHA + 1% AA, MMA + 1% AA and the base case with only MMA/2-EHA.

The formation of homogeneous and uniform membranes requires the adequate mixing of polymer powder, sand, cement and water. Each redispersible powder is characterized by a different water demand. As already anticipated in paragraph 3.1.2, powders sprayed in acidic conditions require a higher amount of water with respect to the powder sprayed at basic conditions, due to the presence of –COOCO$^-$ groups which have lower hydrophilicity. For instance, the sample containing styrene and 1% of acrylic acid (*SI*) requires 30% of water if sprayed in acidic conditions compared to the 27% required by the same dispersion sprayed in basic conditions.

In principle, the more hydrophilic the powder, the less amount of water is needed to redisperse it and form a uniform membrane. This is the case of powders synthesized with methyl methacrylate, which is more hydrophilic with respect to styrene and so requires less water, as shown in Figure 19.

Homogenous membranes could be obtained from all the samples and their surface roughness was comparable to the reference membrane provided by AkzoNobel (Figure 18), even if ours resulted slightly stickier and the trowel-ability could be improved.

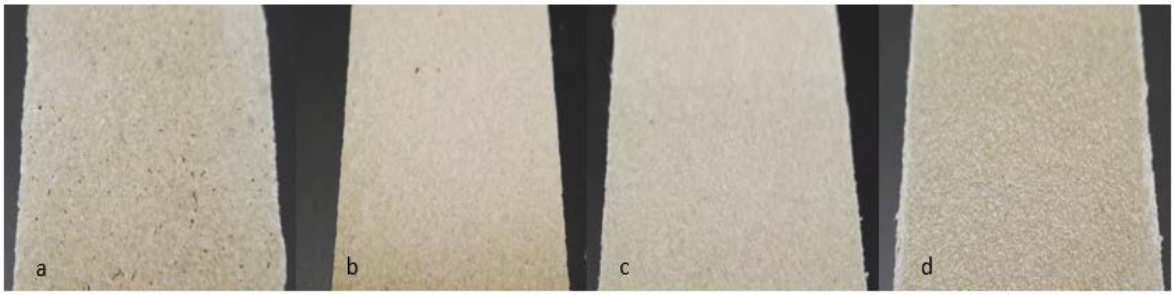

Figure 18. Membranes obtained from samples *S1* (a), *S2* (b) and *S3* (c) compared with the reference (d) from AkzoNobel.

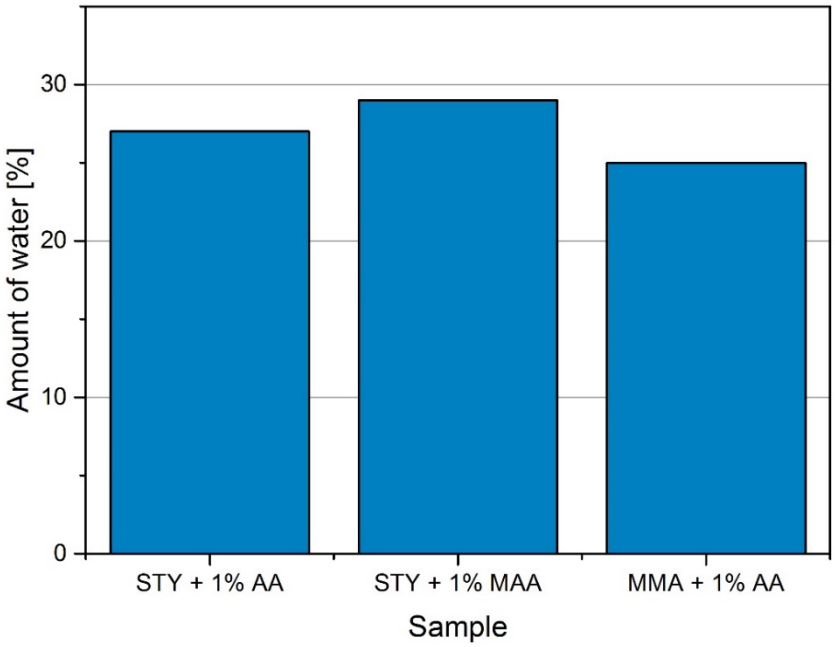

Figure 19. Amount of water needed to form an applicable polymer-cement membrane for the sample containing 1% AA/MAA with STY and MMA.

4.2 Core-shell polymer particles

4.2.1 Synthesis

In order to identify the thickness showing the best performance during spray-drying and giving the most redispersible powder and resisting membrane, core-shell particles have been synthesized having different shell thicknesses, ranging from 2.5 to 20 nm for the ultra-thin (*Sf*) and thick shell (*Sd*) samples, respectively, as sketched in Figure 20. The final particle size, the PDI, the solid content, the zeta potential and the glass transition temperature for the latices synthesized using STY/2-EHA are reported in Table 7. Moreover, the particles characterized by medium shell thickness have been synthesized with increasing styrene content in the shell ranging from 80% to 90% and 99% for samples *Sa*, *Sb* and *Sc*, respectively. It is worth noting that the increase of styrene content in the shell progressively leads to harder and more hydrophobic surfaces. This can certainly have an influence on the spray-ability and the subsequent redispersion of the powders, as will be discussed later on. A content of 80% STY in the shell was then chosen for all the other shell thicknesses, as this value turned out to be the best performing percentage. In order to verify the effect that a larger particle size may have on the spray-drying performances and on the subsequent redispersibility and membrane formation, a sample characterized by ultra-thin shell was synthesized at two different particle sizes (sample *Sf* and *SfL*). This was made by lowering the total percentage of stabilizer inside the system. Moreover, one part of the reduced amount of stabilizer was added at the beginning of the reaction as initial charge, and the other part was fed in time.

Once the optimal shell thickness was identified, styrene was substituted with methyl methacrylate to study the influence of the shell hydrophilicity. This is the case of samples *Ma* and *Mb*, respectively characterized by thin and ultra-thin shell. The final particle size, the PDI, the solid content, the zeta potential and the glass transition temperature for these samples are reported in Table 8.

In order to further enhance the repulsion between the particles, acrylic acid was then added onto the shell surface. This is the case of samples *SeI* and *MaI*, characterized by a thin shell with the addition of 1% AA, which resulted to be the optimal percentage of acid, as reported in Paragraph 4.1.

For syntheses using STY/2-EHA, the obtained particle size is in the range between 250 and 472 nm and the corresponding distributions are all characterized by low values of PDI. Instead, in the case of MMA/2-EHA, larger particles, in the range between 487 and 819 nm, were obtained. Such a difference in particle size has to be imputed to the fact that the stabilizer MAPTAC is fed in time when using MMA rather than fully added at the beginning as with STY, thus leading to larger particles. Sample *MaI* is the only one showing a high value

of PDI. Again, this can be attributed to the phenomenon of secondary nucleation, as mentioned in Paragraph 4.1.1.

As in the case of particles containing carboxyl groups in the previous paragraph, particle size and instantaneous conversion were monitored every hour. Also in this case, the curves show similar trend and shape for all reactions. A typical example for samples synthesized with STY/2-EHA is shown in Figure 21: as expected, both the particle size and the conversion show a rapid increase in the beginning, which gets slower after about 4 hours reaction time due to the progressive monomer depletion. Again, the instantaneous conversion of samples prepared with MMA/2-EHA shows instead a flatter profile representative of higher reactivity, as shown in Figure 22. In this case, the peak shown by the particle size at 4 hour is most probably due to an experimental error resulting in a high PDI value characterizing this specific sample.

Shell geometry	Thick	Medium			Thin	Ultra-thin	Ultra-thin (larger)	Thin + AA
Sample name	*Sd*	*Sa*	*Sb*	*Sc*	*Se*	*Sf*	*SfL*	*SeI*
Size [nm]	321	295	304	288	275	250	472	252
PDI	0.04	0.01	0.03	0.02	0.02	0.02	0.03	0.01
Solid content [%]	36.39	33.07	33.43	34.15	31.78	28.82	29.33	29.80
ζ potential [mV]	44.3	47.7	54.5	51.8	45.3	48.3	44.6	29.1
T_g [°C]	-25.0	-19.5	-27.6	-24.2	-25.6	-22.9	-22.9	-24.1

Table 7. Final particle size, PDI, solid content, ζ potential and T_g of the latices for core-shell particles synthesized with STY/2-EHA.

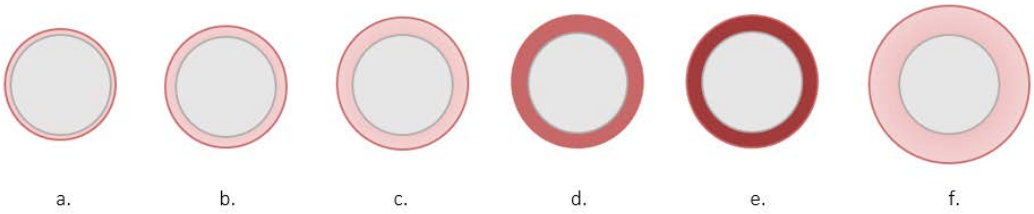

Figure 20. Different core-shell particle geometries. (a) Ultra-thin, (b) thin, and (c) medium shell particles with a styrene content of 80% in the shell. (d) Medium shell particles with a styrene content of (d) 90% and (e) 99% in the shell. (f) Thick shell particle.

Shell geometry	Thin	Ultra-thin	Thin + AA
Sample name	*Ma*	*Mb*	*Mal*
Size [nm]	571	487	819
PDI	0.06	0.04	0.2
Solid content [%]	38.56	37.63	38.78
ζ potential [mV]	31.1	39.6	35.6
T_g [°C]	-24.1	-21.3	-24.7

Table 8. Final particle size, PDI, solid content, ζ potential and T_g of the latices for core-shell particles synthesized with MMA/2-EHA.

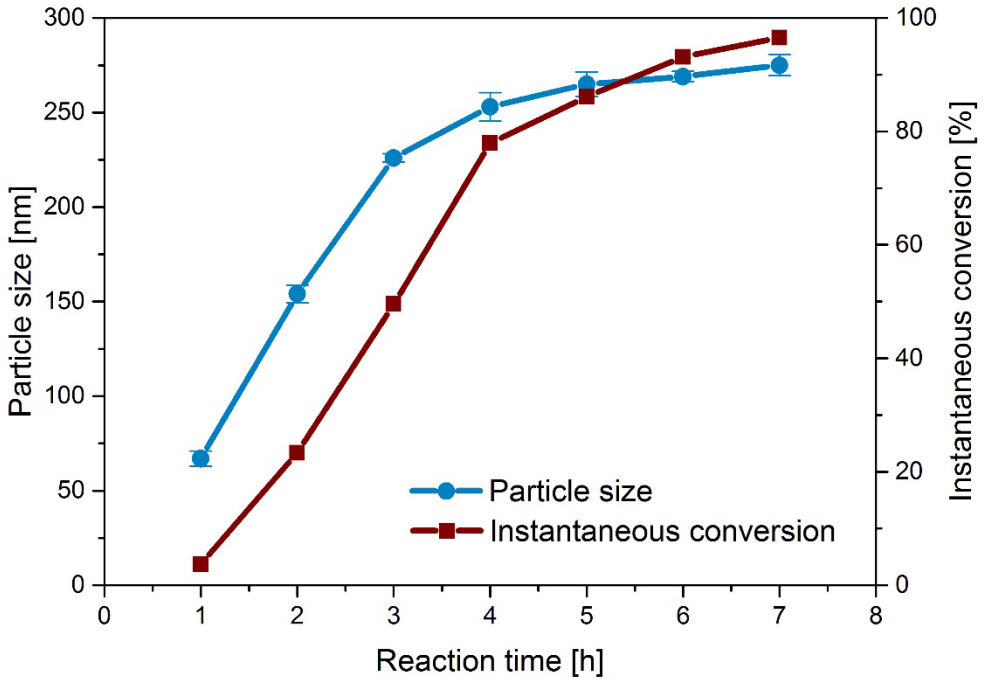

Figure 21. Particle size and instantaneous conversion over time of sample *Se*.

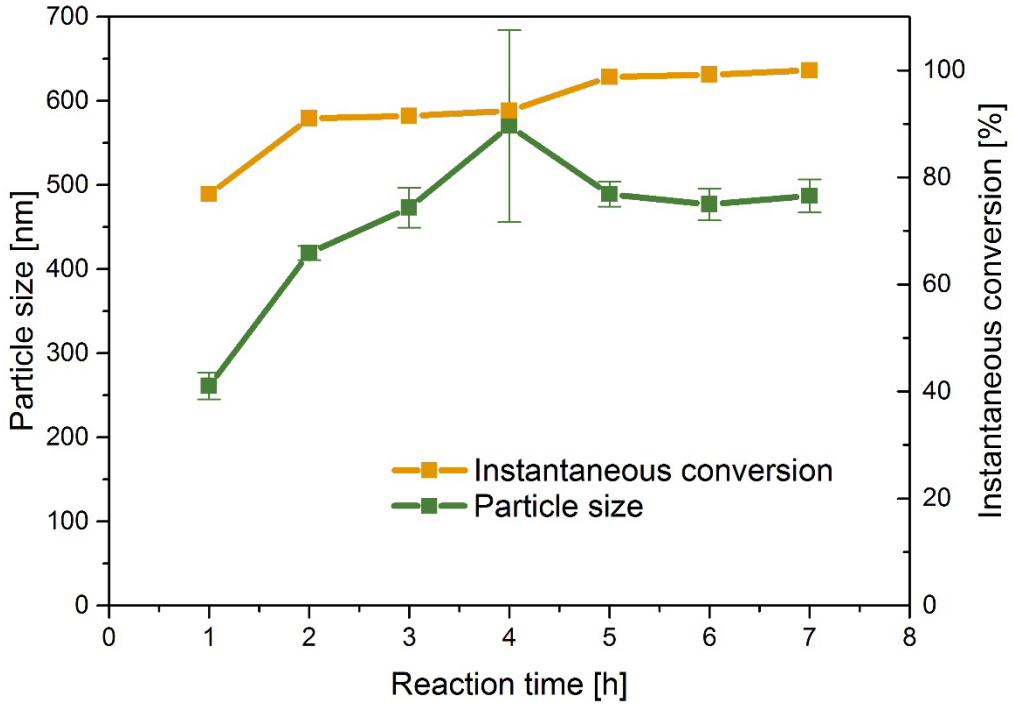

Figure 22. Particle size and instantaneous conversion over time of sample *Mb*.

All samples show positive values of zeta potential at neutral pH, in the range between 51.8 and 29.1 mV. As previously reported, this is due to the presence of MAPTAC as surfactant, which provides positive surface charge. During the reaction, the particle composition was monitored by measuring the NMR spectra of the samples taken hourly. In particular, the mass fraction of 2-EHA in every sample was evaluated by calculating the integral of the spectra. As it can be noticed in Figure 23, during the feed of the core mixture the composition stays roughly the same. Instead, when the shell feed is switched on after 4 hours, a general trend towards the decrease of incorporated 2-EHA can be observed as the shell feed has higher styrene content. Figure 23 reports the variation of 2-EHA composition in time for sample *Sa*, compared to the curve representing the cumulative polymer composition corresponding to the fed monomer mixture assuming complete conversion. It is clearly visible that higher styrene content in the shell feed leads to lower 2-EHA percentage in the particle, resulting in a higher shell T_g. The NMR results for all samples and their evaluation are explained in Section C.1.

After the synthesis was completed, final characterization of each sample was performed and the estimated glass transition temperatures are shown in Table 7 and 8.

The evaluation of the T_g of the shell is not straightforward as the shell feed was started when the core monomer had a conversion of about 80% to obtain a gradual change in composition. Therefore, there is no sharp variation in the DSC profile as the T_g also changes gradually from the core to the outer region of the shell, where the chain composition resembles the shell feed and the T_g is more than 60 °C. The true T_g value of the shell was

measured by synthesizing a shell-only sample and was found to be around 65 °C for the composition STY/2-EHA of 80/20%. In general, the T_g of the core samples lies below -21 °C, which makes them suitable for the application in waterproofing membranes. To make sure the synthesized latex is usable for waterproofing membranes, the ability to form a film has been tested. As expected, all latices were film-forming after synthesis used as is, even when a thick shell was present.

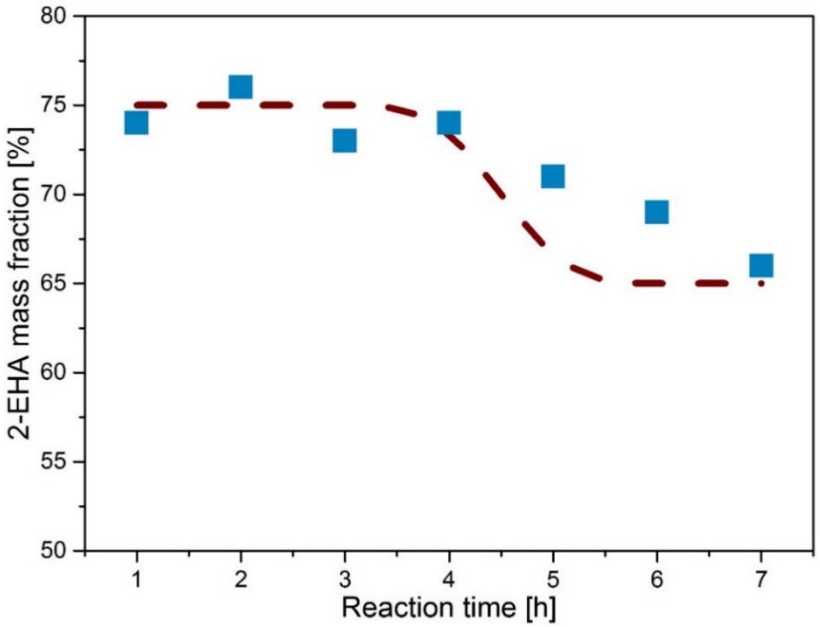

Figure 23. Mass fraction of 2-EHA in the polymer particles for sample *Sa* during the reaction. The dashed curve represents the cumulative polymer composition corresponding to the fed monomer mixture assuming complete conversion.

4.2.2 Spray drying and redispersibility

All the latices used did not show aggregation before being processed into the spray-dryer. All samples containing STY/2-EHA could be spray-dried using a PvOH content of 15% with respect to the polymer and dry powders were obtained. Table 9 summarizes the different samples and their spray-drying behavior. For samples containing MMA/2-EHA, fine powders were obtained from all the dispersions, using 12% of PvOH with respect to the polymer. All samples show no-caking properties. Having a look at the T_g values in Table 7 and 8, it is possible to notice that the spray-ability of the samples is good despite having a low T_g. The core-shell structure, therefore, improves the spray-ability while retaining film-forming properties. This is supported by the fact that a reference sample consisting only of core monomer with no shell could not be spray-dried.

Sample	*Sa*	*Sb*	*Sc*	*Sd*	*Se*	*Sf*	*SfL*	*Sel*	*Ma*	*Mb*	*Mal*
Powder properties	m	m	m	f	f	f	f	f	f	f	f

Table 9. Results of the visual analysis of the spray-dried polymer latices with STY/2-EHA. Powder properties range from fine (f) to medium (m).

Redispersibility was measured to analyze the behavior of the dried polymer powders in water. In principle, it was possible to redisperse all the samples by stirring them and none of them formed immediately large polymer aggregates. After resting for 24h, some powders settled, and the supernatant had different clearness depending on the sample. The redispersibility was visually assessed and the results are shown in Table 10. Once again, the results show that good spray-ability does not necessarily mean the dried powder is well redispersible. In this case, also the hydrophobicity of the shell comes into play. As a harder shell has a higher styrene content, its hydrophobic nature can lead to a more difficult wetting, which makes it difficult to redisperse them in water. On the other hand, when a thin or ultra-thin shell is present, redispersibility improves. Furthermore, when styrene is replaced by methyl methacrylate, its higher hydrophilicity makes the powder more prone to redispersion. This was verified in the redispersion of sample *Mb*, where the combination of an ultra-thin shell with the use of MMA leads to the best redispersion ability.

Sample	*Sa*	*Sb*	*Sc*	*Sd*	*Se*	*Sf*	*SfL*	*Sel*	*Ma*	*Mb*	*Mal*
Redispersibility	gr	mr	mr	gr	gr	mr	gr	gr	gr	vgr	gr

Table 10. Results of the visual analysis of the redispersed polymer powders samples which are classified as very good (vgr), good (gr) and medium (mr).

4.2.3 Crack-bridging and polymer-cement compatibility

Results of expansion-by-crack tests performed on samples *Sa*-*Sf* are shown in Figure 24 and show a similar trend for all tested samples. At temperatures above 20 °C the performance was low for all samples as the polymer is excessively soft and unable to stabilize the composite material. As the temperature decreases, differences between the samples start to emerge. At all temperatures below 0 °C, the sample with the thinnest shell was showing the largest possible expansion. This is due to the thin shell allowing the particles to interpenetrate each other and form a stable film. However, the further reduction in shell thickness seems not to increase the performances. Indeed, a lower crack-resistance with respect to the thin-shell is shown by the sample with the ultra-thin shell, meaning that such a small shell is not enough to limit particle coalescence during the spray-drying, with consequent loss in performance when forming the membrane. However, when sample characterized by ultra-thin shell was increased in size (sample *SfL*) from 250 nm to 472 nm, crack-bridging properties were visibly enhanced, as can be noticed by looking at Figure 25. In general, sample with the thick shell showed a lower performance with respect to the

medium and thin shell samples. Looking at the medium shell samples with different styrene contents in the shell, one can see that a harder shell has a similar influence as a thick shell. Samples *Sb* and *Sc* with 90% and 99% styrene in the shell, respectively, showed a worse performance than sample *Sa* with 80% styrene in the shell. Again, the harder shell makes it difficult for the polymer particles to interpenetrate each other and, therefore, to form a stable film. In general, the performance of all samples decreased at low temperatures, as the polymer becomes harder and more brittle.

When negative charges were added onto a thin shell particle through the addition of acrylic acid to the synthesis, the resistance to crack of this type of particles was further enhanced with respect to the simple thin shell sample, as shown in Figure 26. Indeed, the addition of a layer of charges onto the particle shell allowed the introduction of electric repulsion which, together with the already present steric repulsion, further reduced the possibility of particles coalescence during the drying operation, thus helping the preservation of the properties of the original latex.

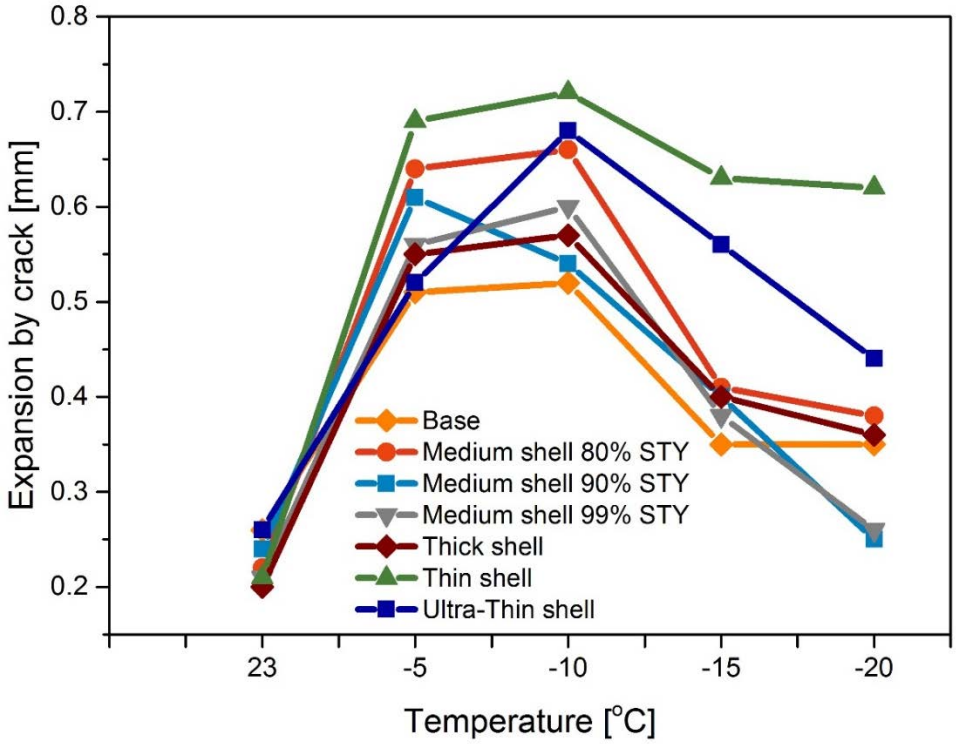

Figure 24. Expansion in millimeters before the membrane breaks at different temperatures for samples *Sa*-*Sf*.

Conversely, crack-bridging tests performed with the samples containing methacrylic acid did not show remarkable results. Indeed, when the crack-bridging properties were compared with the ones obtained from samples of the same type containing styrene, they all showed worse performances, as reported in Figure 27. It is worth noticing that these results prove that a better redispersibility of the powder does not necessarily means higher performances of the membrane.

To get a workable membrane, the polymer powder needs to be mixed homogeneously with sand, cement, and water without coagulation. The dry-mix of all tested samples showed small coagulates of polymer powder but could be mixed properly with water. The amount of water needed to apply a membrane was different from sample to sample, as shown in Figure 29. The percentage shown is with respect to the total dry mixture amount. As expected, sample S_d with the thick shell needed the least amount of water, as a thicker shell leads to less interpenetration and therefore less coagulation when the polymer is redispersed. A harder shell as in sample S_b and S_c, however, leads to more water needed, due to the higher amount of styrene, which is hydrophobic, and is therefore not beneficial. Again, samples synthesized with MMA required lower amount of water compared to the corresponding samples with STY, thanks to the higher hydrophilicity of the monomer with respect to styrene (see sample S_e, S_f, S_{eI} compared to M_a, M_b, M_{aI} respectively).
Nevertheless, as the polymer cement mixtures are planned to be used at the construction site, variances in the amount of water needed do not play a big role compared to their general applicability and crack-bridging properties. Also, less water will be needed if the PvOH amount for spray drying could be reduced as the amount of water is directly dependent on the amount of used PvOH.
The applied membranes were showing a homogeneous but bubbly consistency (see Figure 28). This should be improved further to get a stronger and more waterproof material. As there is little theoretical knowledge about compatibility between cement and polymer powder, it is difficult to draw conclusions and studies of this issue remain mostly trial-and-error. During compatibility experiments with the same cement and similar polymer powder, the compatibility and mixing rheology differed largely.

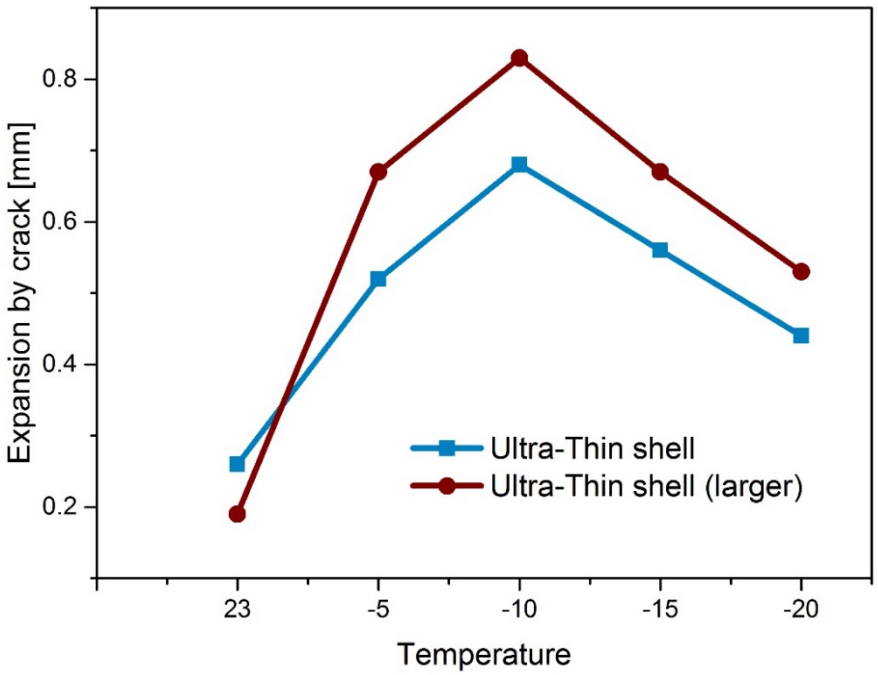

Figure 25. Comparison of the expansion in millimeters before the membrane breaks at different temperatures for sample *Sf* and *SfL*.

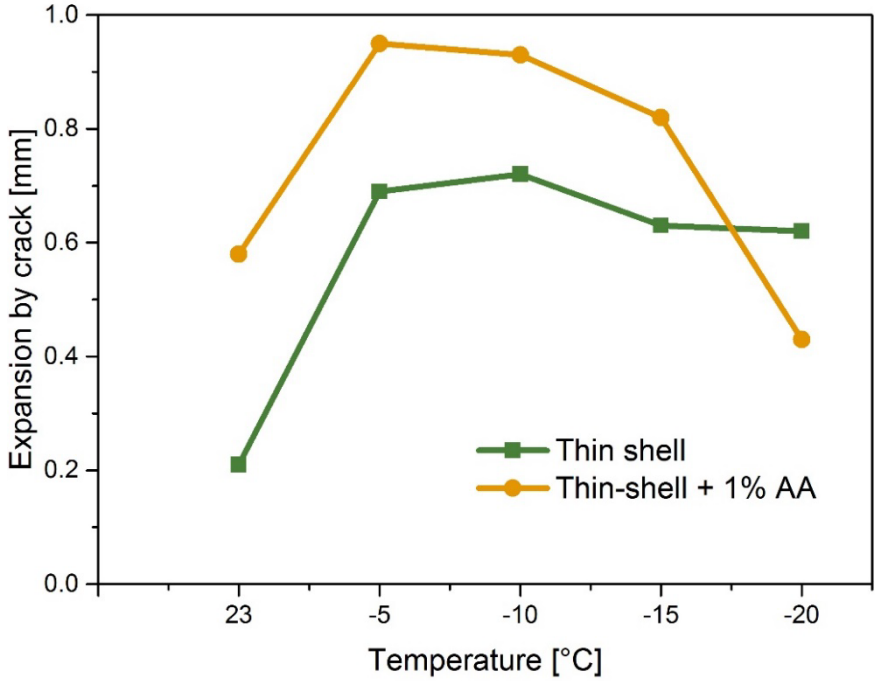

Figure 26. Comparison of the expansion in millimeters before the membrane breaks at different temperatures for samples *Sf* and *SeI*.

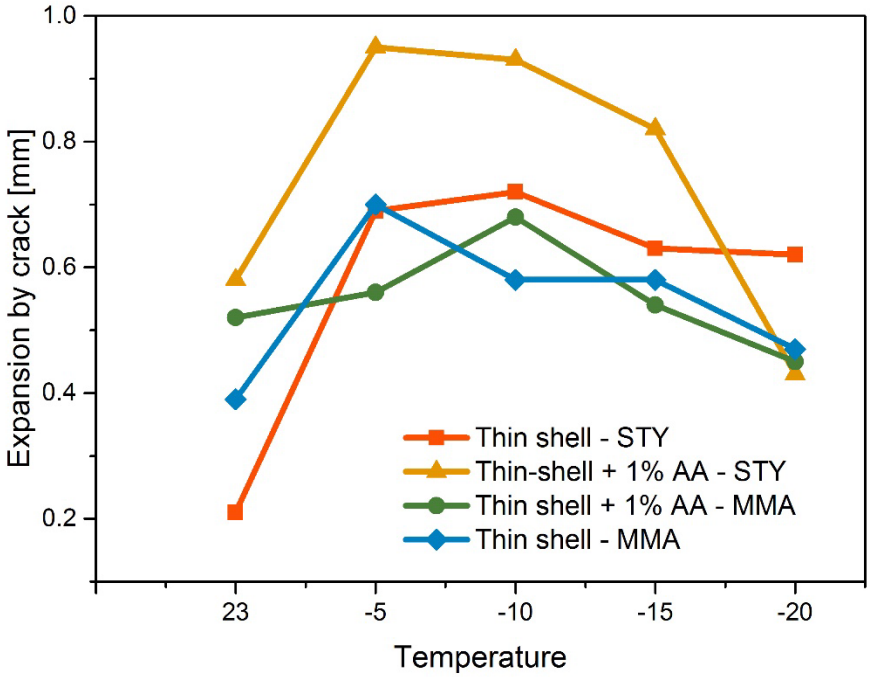

Figure 27. Comparison of the expansion in millimeters before the membrane breaks at different temperatures between samples *Se*, *Sel*, *Ma* and *Mal*.

Figure 28. Membranes obtained from samples *Se* (left) and *Sc* (middle) compared with a reference (right) from AkzoNobel.

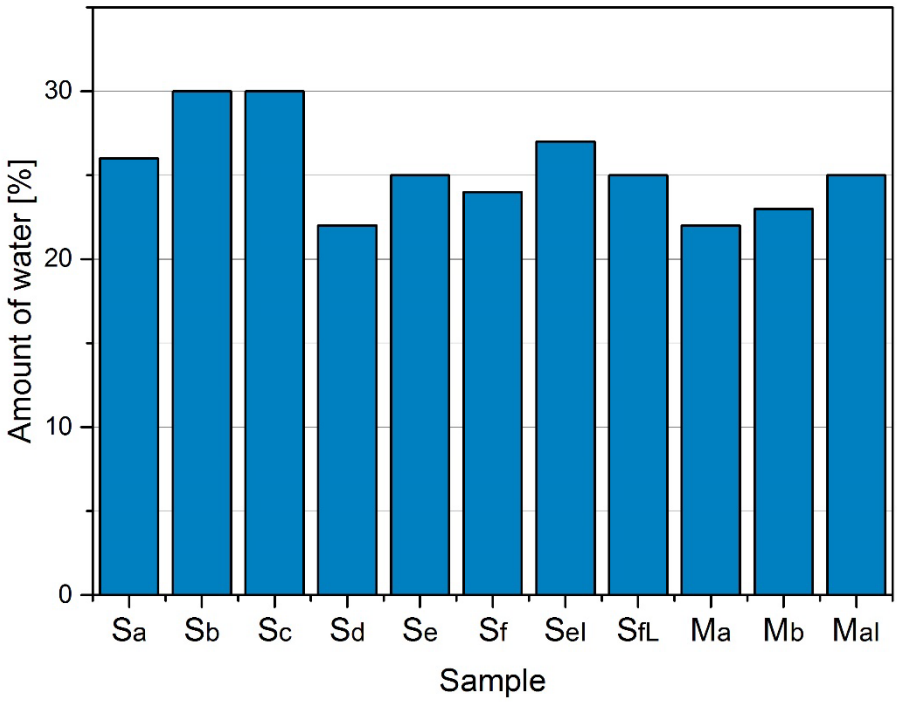

Figure 29. Amount of water needed to form an applicable polymer-cement membrane with core-shell particle latices.

5. Conclusions

It was the aim of this thesis to produce a latex with a glass transition temperature (T_g) around -15 °C able to be spray-dried, and resulting in a water-redispersible powder compatible with cement, to be used in 1-component polymer-cement mortar systems. For this purpose, two different solutions were investigated, in order to study the effect that the addition of carboxyl groups on the particle surface or the core-shell structure of the particles could have on the spray-drying and crack-bridging properties of the resulting product.

Syntheses at high solid content performed *via* free-radical emulsion polymerization using semi-batch conditions under starved operations allowed to have a good control of the product quality in terms of particle size, stability of the dispersion, and copolymer composition. This was verified by NMR measurements which showed, on one hand, a constant composition in time in the case of homogeneous particles, and, on the other hand, for core-shell particles, the expected decrease in the content of 2-ethylhexyl acrylate (2-EHA) in the particles after switching on the shell feed richer in styrene (STY). The average particle size of all the prepared latices was in a range 300-800 nm, a value fulfilling the requirements for optimal spray-drying operation. Furthermore, the measured T_g was within the desired boundaries, thus conferring the latices film-forming ability and ensuring the needed properties for waterproofing membranes.

Spray-drying turned out to be a non-straight-forward treatment, due to its dependence on many operating parameters. For example, the amount of PvOH to be added to the latices prior the drying to limit particle aggregation is a critical parameter which depends on many factors, including the softness of the particles and the type of spray-tower used. In particular, for lab-scale towers the amount of needed PvOH results larger than the one needed for drying the same latices in an industrial-scale tower. All the synthetized samples could be spray-dried and most of them resulted in fine-grained free-flowing powders. In particular, for particles containing carboxyl groups, the addition of 12% of PvOH with respect to the polymer and the pH adjustment to basic conditions resulted in powder with higher crack-bridging properties with respect to the acidic case. For core-shell particles, instead, 15% of PvOH was added with respect to the polymer to achieve good spray-ability. Thus summarizing, both the solutions lead to latices with a good spray-ability despite the very low T_g, while keeping the film-forming properties of the polymer.

None of the powders showed large aggregates or clusters when tested for redispersibility in water. After 24h of standing, some dispersions appeared cloudier than others, indicating a more stable dispersion. In particular, the percentage and the type of acid, the amount and the type of monomer used influenced the redispersibility of the powders. In the case of particles synthesized using STY/2-EHA with addition of acrylic acid (AA), 1% was the best

performing percentage in terms of redispersibility, while when methacrylic acid (MAA) was added no clear trend was observed. As far as the monomer amount is concerned, a higher styrene content leads to a more hydrophobic shell, thus requiring more water to be effectively redispersed. When styrene was substituted with methyl methacrylate (MMA), a decrease in water needed for the redispersion was observed, thanks to the higher hydrophilicity of this monomer.

Crack-bridging tests performed on homogeneous particles with the addition of carboxyl groups showed that powders sprayed in basic pH conditions are more performing with respect to the ones dried in acidic pH conditions. Although a clear trend among the different acid percentages was not found, 1% AA added onto STY/2-EHA particles turned out to be the best acid percentage and copolymer choice. Accordingly, a good redispersibility does not necessary mean good crack resistance, as shown by the samples synthesized containing MMA, whose crack resistance was lower with respect to STY despite the very good redispersibility. The tests performed on core-shell particles showed that a thin shell of 5 nm guarantees good spray-ability while at the same time preserving crack-bridging properties, allowing the particles to interpenetrate each other to form a very stable film. Moreover, it was noticed that the addition of carboxyl groups onto the shell surface and the increment in particle size were able to further enhance the crack resistance of the membrane. Also in this case, although particles synthesized using MMA showed a very good redispersibility, the membranes obtained from these powders showed lower crack-bridging properties with respect to the samples synthesized with STY. Finally, polymer-cement compatibility was acceptable and uniform membranes were obtained.

To conclude, it was possible to synthesize copolymers able to undergo all the necessary steps: synthesis, spray-drying, redispersibility and applicability, for both the particle configurations. While overall performances still have room for improvement, the feasibility and validity of the ideas was thoroughly shown.

6. Recommendations and Outlook

The interesting results obtained in this thesis define the path for future researches focused on further optimization of the product. The investigations on the positive influence of the particle size and the presence of carboxyl groups on the crack-bridging properties of core-shell particles showed that there is still room available for improvement. Besides synthesizing larger thin-shell particles with the presence of carboxyl group onto the surface, the addition of a cross-linker to harden the shell could be worth studying, thanks to the further limitation to the interpenetration that its addition would bring. Furthermore, more studies on the effect and possible advantages that the substitution of styrene with the more hydrophilic methyl methacrylate has on redispersion and crack-bridging properties should be conducted.

In general, the use of a reduced amount of PvOH would be preferable. This could be achieved by moving to a taller drying tower, where higher residence time allows better drying conditions, as already verified by the industrial partner. In addition, the use of additives as substituents for the anti-caking agent would be worth studying, as the agent used in this study may have influence on the powder redispersibility and membrane formation, due to its insolubility in water.

A better knowledge about the polymer-cement compatibility would be helpful as well. Better understanding of the theoretical background would facilitate the choice of the right polymer. For instance, a deep investigation on polymer-cement interactions may also open the way to further studies onto negatively stabilized polymer latices.

To sum up, by taking into account all the considerations made, the optimal material which would be worth studying is represented by a STY/2-EHA core-shell particle structure characterized by a shell of 5 nm hardened with a cross-linking agent and covered by acrylic acid. Further studies on the influence of a different drying tower and the presence of anti-caking agents are as well recommended.

Appendix

A. Synthesis conditions

The exact amounts and conditions of all the syntheses are shown in Tables A.1, A.2, A.3 and A.4.

AA/MAA [%]	0	1	3	5
Sample name	*S*	S_I/S_1	S_{II}/S_2	S_{III}/S_3
MAPTAC (50 wt.%) [g]	18	18	18	18
Water added to MAPTAC [g]	350	350	350	350
V-50 shot [g]	1	1	1	1
Water for V-50 shot [g]	20	20	20	20
Styrene content	35%	35%	35%	35%
Styrene amount [g]	87.5	87.5	87.5	87.5
2-EHA amount [g]	162.5	162.5	162.5	162.5
Monomer mix feed rate [mL min^{-1}]	1.17	1.17	1.17	1.17
Feeding time monomer mix [h]	4	2	2	2
Monomer mix + AA/MAA feed rate [mL min^{-1}]	-	1.19	1.23	1.27
Feeding time monomer mix + AA/MAA [h]	-	2	2	2
V-50 in feed [g]	2	2	2	2
Water for V-50 feed [g]	20	20	20	20
V-50 feed rate [mL min^{-1}]	0.07	0.07	0.07	0.07
Feeding time V-50 [h]	6	6	6	6
Total reaction time [h]	7	7	7	7

Table A.1. Reaction formulations for different AA/MAA percentages using STY/2-EHA monomer mixture.

AA [%]	1	1	1	1	1
Sample name	M_{I1}	M_{I2}	M_{I3}	M_{I4}	M_{I5}
Reactor temperature [°C]	80	80	80	75	70
IC water [g]	350	350	350	350	350
V-50 shot [g]	1	1	1	1	1
Water for V-50 shot [g]	10	10	10	10	10
MMA content	35%	35%	35%	35%	35%
MMA amount [g]	87.50	87.50	87.5	87.5	87.5
2-EHA amount [g]	162.5	162.5	162.5	87.5	87.5
Monomer mix feed rate [mL min^{-1}]	1.15	1.15	1.16	1.15	1.15
Feeding time monomer mix [h]	3	2	4	3	3
Monomer mix AA feed rate [mL min^{-1}]	1.19	1.17	-	1.19	1.19
Feeding time monomer mix AA [h]	1	2	-	1	1
V-50 in feed [g]	2	2	2	2	2
Water for V-50 Feed [g]	20	20	20	20	20
V-50 feed rate [mL min^{-1}]	0.24	0.24	0.24	0.24	0.24
Feeding time V-50 [h]	6	6	6	6	6
MAPTAC in feed [g]	18	18	18	18	18
Water for MAPTAC feed [g]	40	40	40	40	40
MAPTAC feed rate [mL min^{-1}]	0.24	0.24	0.24	0.24	0.24
Feeding time MAPTAC [h]	4	4	4	4	4
Total reaction time [h]	7	7	7	7	7

Table A.2. Reaction formulations for 1% AA using MMA/2-EHA monomer mixture in different feeding combination, timing and reactor temperature conditions.

Shell geometry	Medium			Thick	Thin	Ultra-thin	Thin + 1% AA
Sample	*Sa*	*Sb*	*Sc*	*Sd*	*Se*	*Sf*	*SeI*
MAPTAC (50 wt.%) [g]	15.12	15.12	15.12	16.6	13.6	13	13.6
Water added to MAPTAC [g]	370	370	370	370	370	370	370
V-50 shot [g]	1	1	1	1	1	1	1
Water for V-50 shot [g]	10	10	10	10	10	10	10
Styrene content core	25%	25%	25%	25%	25%	25%	25%
Styrene amount core [g]	42	42	42	42	42	42	42
2-EHA amount core[g]	126	126	126	126	126	126	126
Core feed rate [mL min^{-1}]	1.05	1.05	1.05	1.05	1.05	1.05	1.05
Feeding time core [h]	3	3	3	3	3	3	3
Styrene content shell	80%	90%	99%	80%	80%	80%	80%
Styrene amount shell [g]	33.6	37.8	41.6	50.4	16.8	8.8	16.8
2-EHA amount shell [g]	8.4	4.2	0.42	12.6	4.2	2.2	4.2
AA in the shell [%]	-	-	-	-	-	-	1
Shell feed rate [mL min^{-1}]	0.77	0.77	0.77	1.16	0.39	0.2	0.43
Feeding time shell [h]	1	1	1	1	1	1	1
V-50 in feed [g]	2	2	2	2	2	1.41	1.6
Water for V-50 feed [g]	20	20	20	20	20	40	30
V-50 feed rate [mL min^{-1}]	0.07	0.07	0.07	0.07	0.07	0.07	0.1
Feeding time V-50 [h]	6	6	6	6	6	6	6
Total reaction time [h]	7	7	7	7	7	7	7

Table A.3. Reaction formulations for different core-shell particles for samples using STY/2-EHA. For geometries, refer to Figure 20.

Shell geometry	Thin	Ultra-thin	Thin + 1% AA
Sample name	*Ma*	*Mb*	*Mal*
IC water [g]	330	330	330
V-50 shot [g]	1	1	1
Water for V-50 shot [g]	10	10	10
MMA content core	25%	25%	25%
MMA amount core [g]	56	56	56
2-EHA amount core[g]	168	168	168
Core feed rate [mL min^{-1}]	1.04	1.04	1.04
Feeding time core [h]	4	4	4
MMA content shell	80%	80%	80%
MMA amount shell [g]	16.8	8.8	16.8
2-EHA amount shell [g]	4.2	2.2	4.2
AA in the shell [%]	-	-	1
Shell feed rate [mL min^{-1}]	0.38	0.2	0.42
Feeding time shell [h]	1	1	1
V-50 in feed [g]	2	2	2
Water for V-50 feed [g]	31	31	31
V-50 feed rate [mL min^{-1}]	0.1	0.1	0.1
Feeding time V-50 [h]	6	6	6
MAPTAC in feed [g]	17.6	17	17.6
Water for MAPTAC feed [g]	30	30	30
MAPTAC feed rate [mL min^{-1}]	0.16	0.155	0.157
Feeding time MAPTAC [h]	5	5	5
Total reaction time [h]	7	7	7

Table A.4. Reaction formulations for different core-shell particles for samples using MMA/2-EHA.

B. Methods

B.1 Evaluating DSC plots

To estimate the T_g, the inflection point of the heat flow curve is used. In case of a core-shell morphology of the particles, a second inflection zone at higher temperatures corresponding to the T_g of the shell can be observed.

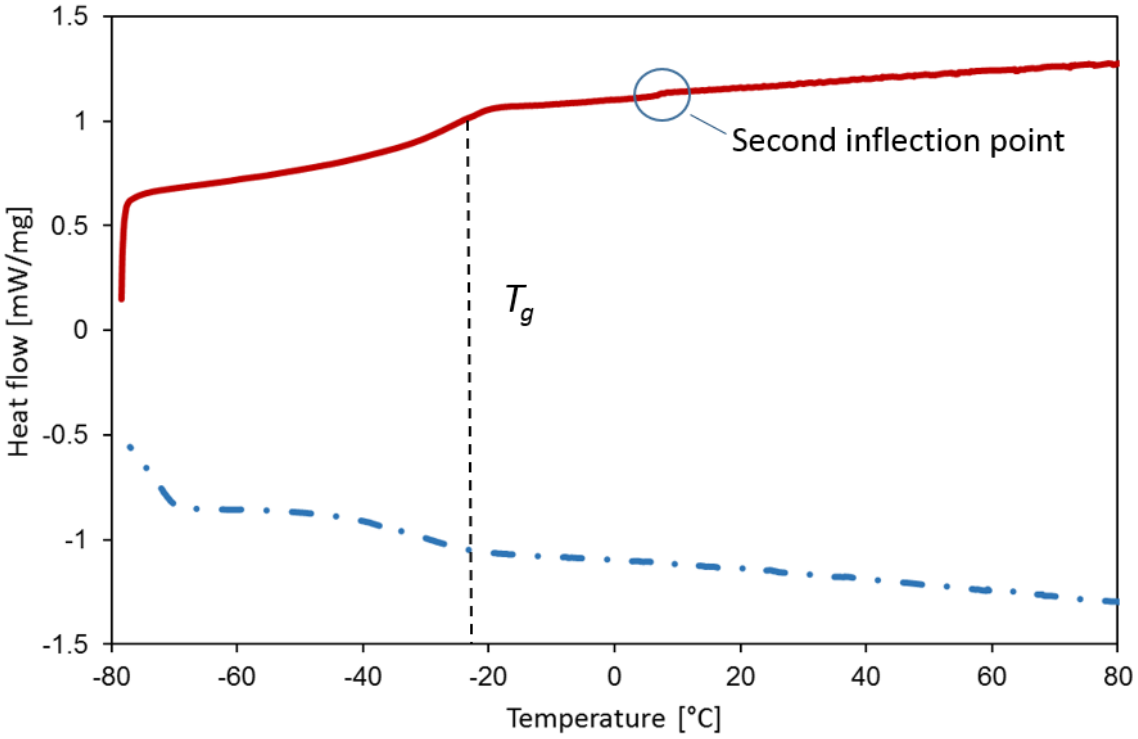

Figure B.1. A typical DSC plot (sample *a*) with the resulting T_g at the inflection point.

B.2 NMR spectra

In order to evaluate the copolymer composition, NMR spectra of the copolymer composed by STY (or MMA) and 2-EHA have been studied. Figure B.2 shows the spectra of 2-EHA monomer (red curve), STY monomer (black curve) and STY/2-EHA copolymer (green curve). By integrating the peaks and comparing the integrals of the peaks, the ratio corresponding to the percentage of 2-EHA present in the copolymer could be calculated. The number and the position of the peaks, corresponding to the hydrogen atoms inside the molecule, allow to identify each single component. For instance, STY is characterized by the presence of four hydrogens of the aromatic ring represented by the peaks at a shift of 7 ppm and by the three peaks at 6.5, 5.5 and 4.5 ppm shift corresponding to the three hydrogens of the double bond. In the same way, 2-EHA can be identified by the three hydrogens of the unsaturated bond, by the one at 4 ppm shift corresponding to the hydrogen near the oxygen, and by the hydrogens of the aliphatic chain in the region 0.5-2 ppm. Once the copolymer is formed, the double bonds disappear, and so do the hydrogen and the corresponding peaks.

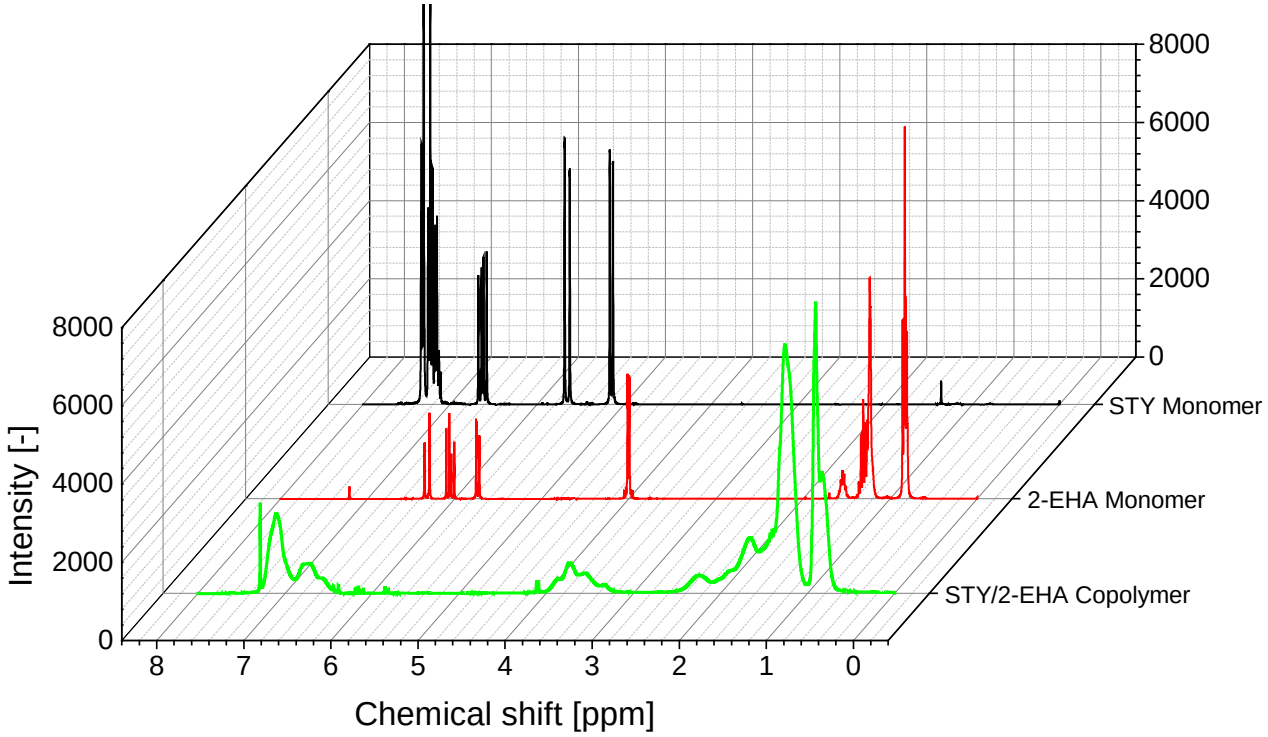

Figure B.2. NMR spectra of 2-EHA monomer (red curve), STY monomer (black curve) and STY/2-EHA copolymer (green curve).

B.3 Crack-bridging test sample preparation

A sketch of the sample preparation procedure for the crack-bridging test is shown in Figure B.3

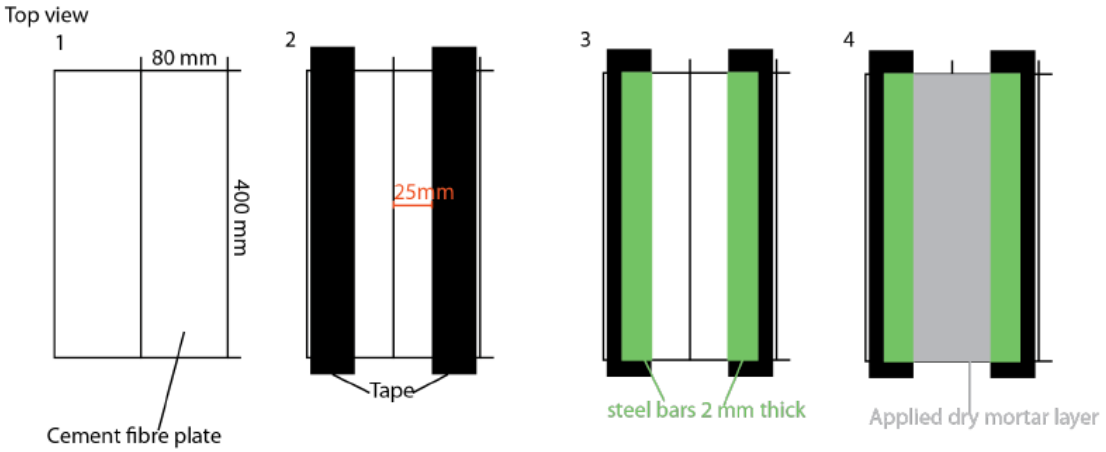

Figure B.3. Sketch of membrane preparation procedure for the crack-bridging test.

C. Synthesis results

Latex properties during synthesis are shown in Tables C.2 and C.3, measurements of the resulting core-shell particle latices are shown in Table C.1.

Sample	Zeta Potential [mV]	pH
Sa	48.8	6.75
Sb	54.4	6.32
Sc	51.8	6.69
Sd	50.9	6.75
Se	50.8	6.69
Sf	48.3	6.83
Sel	29.1	5.81
Ma	31.1	7.75
Mb	39.6	7.38
Mal	35.6	6.27

Table C.1. Surface zeta potential, pH value and film-forming abilities of synthesized latices.

	Sample	1h	2h	3h	4h	5h	6h	final
Solid content [%]	0% AA/MAA *S*	3.36	10.60	20.86	30.39	36.43	38.13	39.07
Inst. conversion [%]		9.87	35.59	59.38	74.80	90.97	95.87	98.35
Particle size [nm]		104	178	226	262	282	287	285
PDI		0.04	0.02	0.02	0.02	0.02	0.02	0.01
Solid content [%]	1% AA *S_I*	3.33	10.89	20.69	27.02	35.61	39.55	40.40
Inst. conversion [%]		7.69	36.80	77.93	78.70	88.37	99.1	100
Particle size [nm]		85	178	228	257	271	281	284
PDI		0.02	0.02	0.02	0.02	0.04	0.04	0.02
Solid content [%]	3% AA *S_{II}*	3.97	10.42	19.08	25.87	36.26	38.97	39.23
Inst. conversion [%]		12.34	34.85	71.18	74.55	89.17	96.61	97.28
Particle size [nm]		94	186	228	254	294	305	333
PDI		0.03	0.05	0.02	0.02	0.06	0.05	0.09
Solid content [%]	5% AA *S_{III}*	3.29	10.60	20.17	29.90	37.95	41.39	41.26
Inst. conversion [%]		7.41	35.59	75.74	86.45	92.63	100	100
Particle size [nm]		78	171	219	244	281	302	301
PDI		0.02	0.02	003	0.02	0.04	0.01	0.02
Solid content [%]	1% MAA *S_1*	3.17	8.68	17.47	27.41	37.80	40.31	40.77
Inst. conversion [%]		6.53	27.60	64.43	79.34	93.15	100	100
Particle size [nm]		89	185	248	283	342	360	356
PDI		0.06	0.05	0.07	0.04	0.1	0.1	0.1
Solid content [%]	3% MAA *S_2*	2.85	9.56	18.34	26.94	35.62	39.08	39.24
Inst. conversion [%]		4.21	31.27	68.08	77.88	87.52	96.89	97.31
Particle size [nm]		88	189	238	252	309	301	288
PDI		0.05	0.03	0.01	0.03	0.1	0.04	0.03
Solid content [%]	5% MAA *S_3*	3.07	10.46	18.46	28.80	38.30	40.12	40.32
Inst. conversion [%]		5.81	35.01	65.58	83.06	93.52	98.62	99.14
Particle size [nm]		88	174	214	240	280	294	304
PDI		0.02	0.01	0.02	0.01	0.03	0.03	0.05

Table C.2. Conversion and particle size results during synthesis for sample with STY/2-EHA and AA/MAA.

	Sample	1h	2h	3h	4h	5h	6h	final
Solid content [%]	*MI1*	12.60	23.19	31.62	37.16	38.02	37.96	38.19
Inst. conversion [%]		83.49	92.16	97.22	98.07	100	100	100
Particle size [nm]		205	258	317	383	515	563	413
PDI		0.05	0.04	0.05	0.08	0.2	0.2	0.2
Solid content [%]	*MI2*	12.36	23.59	30.85	37.41	38.42	38.14	38.73
Inst. conversion [%]		81.89	93.84	94.37	97.44	100	100	100
Particle size [nm]		297	438	478	672	445	643	430
PDI		0.06	0.05	0.1	0.3	0.2	0.3	0.2
Solid content [%]	*MI3*	12.54	23.69	31.69	37.83	38.95	38.72	39.06
Inst. conversion [%]		82.46	93.65	96.87	98.58	100	100	100
Particle size [nm]		695	333	227	187	185	194	214
PDI		0.2	0.2	0.3	0.8	0.3	0.4	0.4
Solid content [%]	*MI4*	14.31	34.34	31.17	37.41	38.73	38.74	39.14
Inst. conversion [%]		95.6	92.79	95.77	97.44	100	100	100
Particle size [nm]		339	480	447	394	436	462	384
PDI		0.06	0.14	0.08	0.26	0.38	0.44	0.3
Solid content [%]	*MI5*	11.05	24.05	31.45	37.37	38.23	38.34	39.17
Inst. conversion [%]		72.5	95.76	96.29	97.33	100	100	100
Particle size [nm]		295	237	210	201	226	204	204
PDI		0.02	0.31	0.29	0.3	0.41	0.3	0.29

Table C.3. Conversion and particle size results during synthesis for sample with MMA/2-EHA and 1% AA at different operating conditions.

	Sample	1h	2h	3h	4h	5h	6h	final
Solid content [%]	*Sa*	2.15	7.14	14.77	22.57	27.40	31.97	33.07
Inst. conversion [%]		1.86	25.93	44.82	71.67	76.42	90.30	93.57
Particle size [nm]		60.5	146	234	245	275	290	295
PDI		0.07	0.09	0.04	0.02	0.02	0.04	0.01
Solid content [%]	*Sb*	2.30	7.52	15.97	23.58	27.83	31.44	33.43
Inst. conversion [%]		3.01	26.42	48.98	75.32	77.90	89.03	95.20
Particle size [nm]		64	155	229	263	275	302	304
PDI		0.06	0.1	0.06	0.02	0.05	0.08	0.03
Solid content [%]	*Sc*	2.29	8.51	16.37	24.04	27.85	31.91	34.15
Inst. conversion [%]		2.99	30.97	50.27	76.71	77.70	90.06	96.91
Particle size [nm]		-	141	206	239	258	271	288
PDI		-	0.09	0.02	0.05	0.01	0.03	0.02
Solid content [%]	*Sd*	2.77	8.29	14.09	21.73	26.50	31.54	34.39
Inst. conversion [%]		5.40	29.32	42.17	68.64	76.20	83.91	91.93
Particle size [nm]		58	142	213	260	280	301	321
PDI		0.07	0.04	0.02	0.01	0.03	0.02	0.04
Solid content [%]	*Se*	2.25	6.74	16.06	24.30	28.14	30.72	31.78
Inst. conversion [%]		3.72	23.33	49.52	77.96	86.10	93.11	96.83
Particle size [nm]		67	154	226	253	256	269	275
PDI		0.06	0.03	0.01	0.03	0.02	0.01	0.02
Solid content [%]	*Sf*	4.69	7.62	14.52	22.02	25.92	27.89	28.82
Inst. conversion [%]		24.58	28.28	45.45	72.18	83.95	90.69	93.88
Particle size [nm]		74	165	226	240	245	250	250
PDI		0.09	0.03	0.03	0.01	0.01	0.02	0.02
Solid content [%]	*SeI*	2.32	7.94	14.7	21.61	25.98	28.83	29.8
Inst. conversion [%]		4.65	29.29	45.55	69.90	80.09	88.24	91.37
Particle size [nm]		75	172	223	242	252	250	252
PDI		0.04	0.03	0.02	0.01	0.03	0.02	0.01
Solid content [%]	*Ma*	11.55	22.57	29.98	35.43	38.15	38.45	38.56
Inst. conversion [%]		79.38	92.68	94.54	94.71	98.44	99.98	100
Particle size [nm]		309	443	475	-	571	559	571
PDI		0.1	0.06	0.06	-	0.1	0.05	0.06
Solid content [%]	*Mb*	11.19	22.17	29.04	34.62	37.39	37.27	37.63
Inst. conversion [%]		76.84	91	91.45	92.43	98.78	99.18	100
Particle size [nm]		261	419	473	-	489	477	487
PDI		0.06	0.02	0.05	-	0.03	0.04	0.04

Solid content [%]	*MaI*	10.66	22.38	29.52	34.32	38.52	38.69	38.78
Inst. conversion [%]		72.86	91.85	92.99	91.56	98.83	100	100
Particle size [nm]		303	444	538	516	580	674	819
PDI		0.09	0.03	0.2	0.04	0.06	0.2	0.2

Table C.4. Conversion and particle size results during synthesis for core-shell particles samples.

C.1 NMR results

Table C.5 shows the full NMR results for the studied samples.

Sample	2h	3h	4h	5h	6h	7h
Sa	0.72	0.70	0.72	0.71	0.69	0.68
Sb	0.71	0.70	0.73	0.74	0.70	0.66
Sc	-	-	0.74	0.75	0.70	0.67
Sd	0.73	0.70	0.71	0.73	0.68	0.65
Se	0.68	0.68	0.72	0.74	0.73	0.72
Sf	0.68	0.68	0.70	0.72	0.73	0.73
SeI	0.67	0.67	0.70	0.72	0.71	0.71
Ma	0.68	0.72	0.73	0.73	0.74	0.75
Mb	0.67	0.71	0.75	0.75	0.73	0.75
MaI	0.63	0.68	0.71	0.75	0.74	0.73
S	0.64	0.62	0.64	0.65	0.66	0.66
SI	0.60	0.62	0.63	0.64	0.65	0.65
SII	0.66	0.63	0.66	0.68	0.67	0.66
SIII	0.64	0.62	0.66	0.67	0.67	0.67
S1	0.69	0.65	0.69	0.69	0.68	0.68
S2	0.70	0.63	0.65	0.67	0.66	0.67
S3	0.67	0.64	0.69	0.68	0.68	0.68
MI1	0.63	0.65	0.66	0.69	0.68	0.67
MI2	0.65	0.65	0.65	0.68	0.66	0.67
MI3	0.68	0.68	0.66	0.68	0.67	0.68
MI4	0.63	0.64	0.66	0.66	0.66	0.66
MI5	0.63	0.66	0.67	0.65	0.65	0.67

Table C.5. Mass fraction of 2-EHA in the samples taken hourly. The samples taken after one hour always had a too low concentration for an accurate evaluation.

References

1. Blackley, D., *Polymer latices.* Science and Technology, 1997. Vol. 2.
2. Takamura, K.K., D; Urban, D, *Polymer dispersions and their industrial applications*. 2002: Willey-VCH
3. Asua, J., *Polymeric dispersions: principles and applications.* Applied Science, 1996.
4. Yamak, H., *Emulsion polymerization: effects of polymerization variables on the properties of vinyl acetate based emulsion polymers*, in *Polymer Science*. 2013, InTech.
5. Asua, J. and H. Schoonbrood, *Reactive surfactants in heterophase polymerization.* Acta Polymerica, 1998. 49(12): p. 671-686.
6. Ayoub, M., *Emulsion copolymerization latices for interior and exterior coatings.* Pigment & Resin Technology. Vol. 26: p. 6-11.
7. De la Cal, J.L., JR; Asua, JM; Buttè, A; Storti, G; Morbidelli, M, *Emulsion polymerization*, in *Handbook of Polymer Reaction Engineering*, J.K. T.Meyer, Editor. 2005, Wiley-VCH
8. Brandrup, J., et al., *Polymer handbook*. Vol. 7. 1989: Wiley New York etc.
9. Van den Boomen, F., *Composition control in emulsion copolymerization*. 1997, Technische Universiteit Eindhoven.
10. Dimitratos, J., G. Elicabe, and C. Georgakis, *Control of emulsion polymerization reactors.* AIChE journal, 1994. 40(12): p. 1993-2021.
11. Jovanović, R. and M. Dube, *Emulsion-based pressure-sensitive adhesives: a review.* Journal of Macromolecular Science, Part C: Polymer Reviews, 2004. 44(1): p. 1-51.
12. Eliseeva, V., et al., *Emulsion polymerization and its applications in industry*. 2012: Springer Science & Business Media.
13. Lalevée, J. and J. Fouassier, *Overview of radical initiation.* Encyclopedia of Radicals in Chemistry, Biology and Materials, 2012.
14. Guyot, A., *Advances in reactive surfactants.* Advances in Colloid and Interface Science, 2004. 108: p. 3-22.
15. Lam, S., et al., *Surfactants in heterophase polymerization: A study of film formation using force microscopy.* Journal of Applied Polymer Science, 1997. 66(1): p. 187-198.
16. Gauthier, C., et al., *Reactive surfactants in heterophase polymerization. XVII. Influence of the surfactant on the mechanical properties and hydration of the films.* Journal of applied polymer science, 2002. 84(9): p. 1686-1700.
17. Guyot, A. and K. Tauer, *Reactive surfactant in emulsion polymerization.* Advances in Polymer Science, 1994. Vol III.
18. Guyot, A., et al., *Reactive surfactants in heterophase polymerization.* Acta Polymerica, 1999. 50(2-3): p. 57-66.
19. Schoonbrood, H. and J. Asua, *Reactive surfactants in heterophase polymerization. 9. Optimum surfmer behavior in emulsion polymerization.* Macromolecules, 1997. 30(20): p. 6034-6041.
20. Unzué, M., et al., *Reactive surfactants in heterophase polymerization. VI. Synthesis and screening of polymerizable surfactants (surfmers) with varying reactivity in high solids*

styrene—butyl acrylate—acrylic acid emulsion polymerization. Journal of Applied Polymer Science, 1997. **66**(9): p. 1803-1820.
21. Wang, X., E. Sudol, and M. El-Aasser, *Mechanism of emulsion polymerization of styrene using a reactive surfactant.* Journal of Polymer Science Part A: Polymer Chemistry, 2001. **39**(18): p. 3093-3105.
22. Tauer, K., et al. *Emulsion polymerization in the presence of polymerizable emulsifiers and surface active initiators*. in *Makromolekulare Chemie. Macromolecular Symposia*. 1990. Wiley Online Library.
23. Swift, G., *Acrylic (and methacrylic) acid polymers.* Encyclopedia of Polymer Science and Technology, 2002. **1**.
24. Morbidelli, M. and P. Arosio, *Polymerization reaction and colloid engineering*. 2016: ETH Zürich.
25. Gordon, J., *Mechanism of emulsion polymerization.* British Polymer Journal, 1970. **Vol. 1**.
26. Baradiaran, M., J. De la Cal, and J. Asua, *Emulsion Polymerization*, in *Polymer reaction engineering*, J. Asua, Editor. 2008.
27. Niu, L., L. Lei, and Z. Xia, *Redispersible polymer powder functionalized with NMA and its adhesive properties in dry-mixed coatings.* Journal of Adhesion Science and Technology, 2013. **27**(13): p. 1432-1445.
28. Pei, Y., et al., *Redispersibility of acrylate polymer powder and stability of its reconstituted latex.* Journal of Dispersion Science and Technology, 2011. **32**(9): p. 1279-1284.
29. Kuehn, H., et al., *Redispersible polymer powder*. 2002: US.
30. Saija, L. and M. Uminski, *Water-redispersible low-Tg acrylic powders for the modification of hydraulic binder compositions.* Journal of Applied Polymer Science, 1999. **71**(11): p. 1781-1787.
31. Walton, D., *Spray-Dried Particle Morphologies.* Developments in Chemical Engineering and Mineral Processing, 2002. **10**(3-4): p. 323-348.
32. Willimann, H. and R. Koelliker, *Redispersible powder and its aqueous dispersion, preparation, process and use*. 2011, Patent: Europe.
33. Zhang, X., et al., *Modeling spray drying of redispersible polyacrylate powder.* Drying technology, 2014. **32**(2): p. 222-235.
34. Thaker, S., et al., *Synthesis and spray drying of water-redispersible polymer.* Drying Technology, 2010. **28**(5): p. 669-676.
35. Chen, X., B. Zheng, and J. Shen, *Morphologies of polymer grains during spray drying.* Drying technology, 2013. **31**(4): p. 433-438.
36. Maa, Y., et al., *The effect of operating and formulation variables on the morphology of spray-dried protein particles.* Pharmaceutical development and technology, 1997. **2**(3): p. 213-223.
37. Pei, Y., et al., *Stabilization mechanism of the reconstituted emulsion of polyacrylate redispersible powder.* Chemical Engineering Communications, 2015. **202**(9): p. 1245-1250.
38. Bressan, M., et al., *Complementi di operazioni unitarie*. Politecnico di Milano.
39. Walton, D. and C. Mumford, *Spray dried products-characterization of particle morphology.* Chemical Engineering Research and Design, 1999. **77**(1): p. 21-38.
40. Gonzalez-Leon, J., et al., *Core− Shell Polymer Nanoparticles for Baroplastic Processing.* Macromolecules, 2005. **38**(19): p. 8036-8044.

41. Hong, L., et al., *Impact of particle size and surface charge density on redispersibility of spray-dried powders.* Colloids and Surfaces A: Physicochemical and Engineering Aspects, 2014. **459**: p. 274-281.
42. Raines, C. and P. Starmer, *Free flowing particles of an emulsion polymer having SiO2 incorporeted therein*. 1991: US.
43. Tsai, M., G. Papsin, and S. Chiou, *A redispersible core-shell polymer powder*. 1995: US.
44. Wang, F., et al., *Synthesis and redispersibility of poly (styrene-block-n-butyl acrylate) core–shell latexes by emulsion polymerization with RAFT agent–surfactant design.* Macromolecules, 2015. **48**(5): p. 1313-1319.
45. Keddie, J., *Film formation of latex.* Materials Science and Engineering: R: Reports, 1997. **21**(3): p. 101-170.
46. Steward, P., J. Hearn, and M. Wilkinson, *An overview of polymer latex film formation and properties.* Advances in colloid and interface science, 2000. **86**(3): p. 195-267.
47. Winnik, M., *Latex film formation.* Current opinion in colloid & interface science, 1997. **2**(2): p. 192-199.
48. Jin, Y., *Interaction between vinyl acetate-ethylene latex stabilized with polyvinyl alcohol and Portland cement.* 2016.
49. Ludwig, I., et al., *Drying and film formation of industrial waterborne latices.* AIChE Journal, 2007. **53**(3): p. 549-560.
50. Du Chesne, A., et al., *Film formation and redispersion of waterborne latex coatings.* Journal of colloid and interface science, 2000. **224**(1): p. 91-98.
51. Felton, L., *Mechanisms of polymeric film formation.* International journal of pharmaceutics, 2013. **457**(2): p. 423-427.
52. Sperry, P., et al., *Role of water in particle deformation and compaction in latex film formation.* Langmuir, 1994. **10**(8): p. 2619-2628.
53. Protzman, T. and G. Brown, *An apparatus for the determination of the minimum film temperature of polymer emulsions.* Journal of Applied Polymer Science, 1960. **4**(10): p. 81-85.
54. Joanicot, M., et al., *Ordering of latex particles during film formation*, in *Trends in Colloid and Interface Science IV*. 1990, Springer. p. 175-183.
55. Afridi, M., et al., *Development of polymer films by the coalescence of polymer particles in powdered and aqueous polymer-modified mortars.* Cement and Concrete Research, 2003. **33**(11): p. 1715-1721.
56. Afridi, M., et al., *Strength and elastic properties of powdered and aqueous polymer-modified mortars.* Cement and Concrete Research, 1994. **24**(7): p. 1199-1213.
57. Saija, L., *Waterproofing of portland cement mortars with a specially designed polyacrylic latex.* Cement and concrete research, 1995. **25**(3): p. 503-509.
58. Wang, R. and P. Wang, *Action of redispersible vinyl acetate and versatate copolymer powder in cement mortar.* Construction and building materials, 2011. **25**(11): p. 4210-4214.
59. Zhao, F., et al., *Preparation and properties of an environment friendly polymer-modified waterproof mortar.* Construction and Building Materials, 2011. **25**(5): p. 2635-2638.
60. Ohama, Y., *Principle of latex modification and some typical properties of latex-modified mortars and concretes adhesion.* Materials Journal, 1987. **84**(6): p. 511-518.

61. Muhammad, N., et al., *Waterproof performance of concrete: A critical review on implemented approaches.* Construction and Building Materials, 2015. **101**: p. 80-90.
62. Schulze, J. and O. Killermann, *Long-term performance of redispersible powders in mortars.* Cement and Concrete Research, 2001. **31**(3): p. 357-362.
63. Fan, X. and L. Niu, *Performance of redispersible polymer powders in wall coatings.* Journal of Adhesion Science and Technology, 2015. **29**(4): p. 296-307.
64. Pecora, R., *Dynamic light scattering measurement of nanometer particles in liquids.* Journal of nanoparticle research, 2000. **2**(2): p. 123-131.
65. Kaszuba, M., et al., *Measuring sub nanometre sizes using dynamic light scattering.* Journal of Nanoparticle Research, 2008. **10**(5): p. 823-829.
66. Xu, R., *Light scattering: A review of particle characterization applications.* Particuology, 2015. **18**: p. 11-21.
67. Kholodenko, A. and J. Douglas, *Generalized Stokes-Einstein equation for spherical particle suspensions.* Physical Review E, 1995. **51**(2): p. 1081.
68. Einstein, A., *Elementare Theorie der Brownschen Bewegung.* Zeitschrift für Elektrochemie und angewandte physikalische Chemie, 1908. **14**(17): p. 235-239.
69. Hunter, R., *Zeta potential in colloid science: principles and applications*. Vol. 2. 2013: Academic press.
70. Zhang, Y., et al., *Zeta potential: a surface electrical characteristic to probe the interaction of nanoparticles with normal and cancer human breast epithelial cells.* Biomedical microdevices, 2008. **10**(2): p. 321-328.
71. Young, R. and P. Lovell, *Introduction to polymers*. 2011: CRC press.